Dear Author

Please use this PDF proof to check the layout of your article. If you would like any changes to be made to the layout, you can leave instructions in the online proofing interface. First, return to the online proofing interface by clicking "Edit" at the top page, then insert a Comment in the relevant location. Making your changes directly in the online proofing interface is the quickest, easiest way to correct and submit your proof.

Please note that changes made to the article in the online proofing interface will be added to the article before publication, but are not reflected in this PDF proof.

If you would prefer to submit your corrections by annotating the PDF proof, please download and submit an annotatable PDF proof by clicking the link below.

Annotate PDF

Article

Immunity

Interleukin-3 coordinates glial-peripheral immune crosstalk to incite multiple sclerosis

Graphical abstract

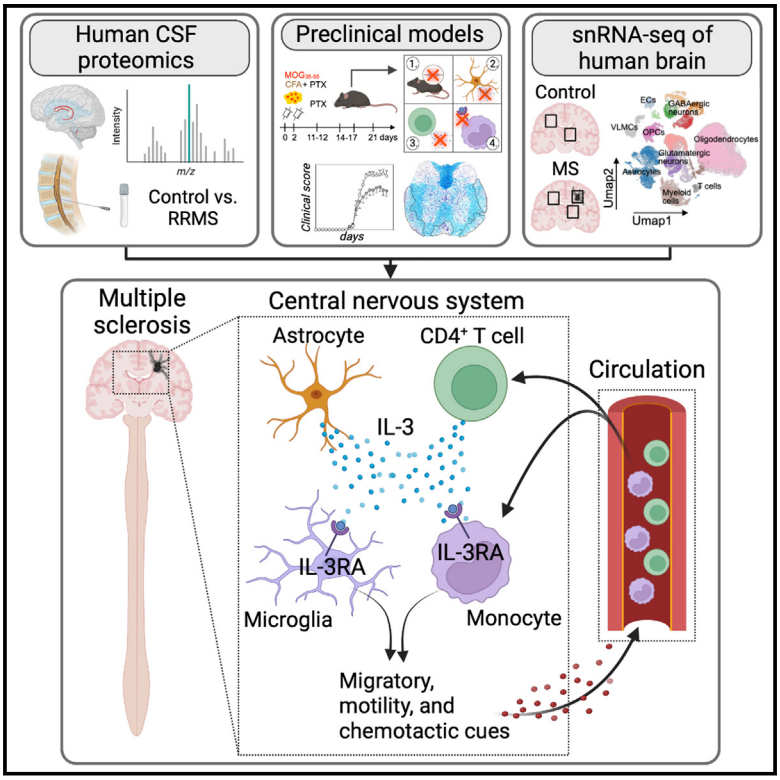

Highlights

- IL-3 is elevated in the CSF of MS patients and associates with disease severity
- IL-3 deletion protects against neuroinflammation and disease in a mouse model of MS
- In the CNS, astrocytes and T cells produce IL-3
- In MS, IL-3 programs *IL3RA*-expressing myeloid cells to generate chemotactic cues

Authors

Máté G. Kiss, John E. Mindur, Abi G. Yates, ..., Panos Roussos, Filip K. Swirski, Cameron S. McAlpine

Correspondence

cameron.mcalpine@mssm.edu

In brief

IL-3 is a multifunction cytokine whose function in neuroinflammation is presently unclear. Kiss et al. reveal that astrocyte- and T cell-sourced IL-3 programs myeloid cells to exacerbate neuroinflammation by inciting a cellular recruitment program that drives the accrual of immune cells in the CNS, worsening MS and its preclinical model.

Kiss et al., 2023, Immunity *56*, 1–13
July 11, 2023
https://doi.org/10.1016/j.immuni.2023.04.013

CellPress

Please cite this article in press as: Kiss et al., Interleukin-3 coordinates glial-peripheral immune crosstalk to incite multiple sclerosis, Immunity (2023), https://doi.org/10.1016/j.immunu.2023.04.013

Immunity

CellPress

Article

Interleukin-3 coordinates glial-peripheral immune crosstalk to incite multiple sclerosis

Máté G. Kiss,[1,2,3,15] John E. Mindur,[3,15] Abi G. Yates,[1,2] Donghoon Lee,[2,4] John F. Fullard,[2,4] Atsushi Anzai,[3] Wolfram C. Poller,[1,3] Kathleen A. Christie,[5,6] Yoshiko Iwamoto,[3] Vladimir Roudko,[7] Jeffrey Downey,[1,3] Christopher T. Chan,[3] Pacific Huynh,[1,2] Henrike Janssen,[1,3] Achilles Ntranos,[8] Jan D. Hoffmann,[1,2] Walter Jacob,[1,2] Sukanya Goswami,[1,2] Sumnima Singh,[1,3] David Leppert,[9] Jens Kuhle,[9] Seunghee Kim-Schulze,[7] Matthias Nahrendorf,[3] Benjamin P. Kleinstiver,[5,6] Fay Probert,[10] Panos Roussos,[2,4,11,12] Filip K. Swirski,[1,3,13,14] and Cameron S. McAlpine[1,2,3,16,*]

[1]Cardiovascular Research Institute and the Department of Medicine, Cardiology, Icahn School of Medicine at Mount Sinai, New York, NY, USA
[2]Friedman Brain Institute and the Nash Family Department of Neuroscience, Icahn School of Medicine at Mount Sinai, New York, NY, USA
[3]Center for Systems Biology and the Department of Radiology, Massachusetts General Hospital and Harvard Medical School, Boston, MA, USA
[4]Center for Disease Neurogenomics and the Icahn Institute for Data Science and Genomic Technology and the Departments of Psychiatry and Genetics and Genomic Sciences, Icahn School of Medicine at Mount Sinai, New York, NY, USA
[5]Center for Genomic Medicine, Department of Pathology, Massachusetts General Hospital, Boston, MA, USA
[6]Department of Pathology, Harvard Medical School, Boston, MA, USA
[7]Human Immune Monitoring Center, Icahn School of Medicine at Mount Sinai, New York, NY, USA
[8]Department of Neurology, Icahn School of Medicine at Mount Sinai, New York, NY, USA
[9]Departments of Medicine, Clinical Research and Biomedicine, University Hospital Basel, University of Basel, Basel, Switzerland
[10]Department of Pharmacology and Department Chemistry, University of Oxford, Oxford, UK
[11]Mental Illness Research Education and Clinical Center, James J. Peters VA Medical Center, New York, NY, USA
[12]Center for Dementia Research, Nathan Kline Institute for Psychiatric Research, Orangeburg, NY, USA
[13]Marc and Jennifer Lipschultz Precision Immunology Institute, Icahn School of Medicine at Mount Sinai, New York, NY, USA
[14]Biomedical Engineering and Imaging Institute, Icahn School of Medicine at Mount Sinai, New York, NY, USA
[15]These authors contributed equally
[16]Lead contact
*Correspondence: cameron.mcalpine@mssm.edu
https://doi.org/10.1016/j.immuni.2023.04.013

SUMMARY

Glial cells and central nervous system (CNS)-infiltrating leukocytes contribute to multiple sclerosis (MS). However, the networks that govern crosstalk among these ontologically distinct populations remain unclear. Here, we show that, in mice and humans, CNS-resident astrocytes and infiltrating CD44^{hi}CD4^{+} T cells generated interleukin-3 (IL-3), while microglia and recruited myeloid cells expressed interleukin-3 receptor-α (IL-3Rα). Astrocytic and T cell IL-3 elicited an immune migratory and chemotactic program by IL-3Rα^{+} myeloid cells that enhanced CNS immune cell infiltration, exacerbating MS and its preclinical model. Multiregional snRNA-seq of human CNS tissue revealed the appearance of *IL3RA*-expressing myeloid cells with chemotactic programming in MS plaques. *IL3RA* expression by plaque myeloid cells and IL-3 amount in the cerebrospinal fluid predicted myeloid and T cell abundance in the CNS and correlated with MS severity. Our findings establish IL-3:IL-3RA as a glial-peripheral immune network that prompts immune cell recruitment to the CNS and worsens MS.

INTRODUCTION

Multiple sclerosis (MS) is a chronic neuroinflammatory disease that affects young adults and remains without cure.[1,2] Instigated by autoimmune reactivity to myelin, MS is clinically characterized by episodes of neurologic disability lasting days or weeks. Clinical symptoms often progress over decades and eventually lead to impaired mobility, reduced cognition, and ultimately paralysis and early death. Pathologically, MS presents as inflammatory neuropil and demyelinated lesions throughout the central nervous system (CNS), which are composed of peripherally derived immune cell infiltrates and resident glial cells including astrocytes and microglia. The presence of ontologically distinct immune and glial cell populations—astrocytes deriving from embryonic neuronal progenitors, microglia from primitive yolk sac hematopoiesis, and peripheral innate and adaptive immune cells from adult bone marrow (BM) hematopoiesis—necessitates tightly controlled communication systems to orchestrate cellular function in this complex inflammatory milieu. Immune

Please cite this article in press as: Kiss et al., Interleukin-3 coordinates glial-peripheral immune crosstalk to incite multiple sclerosis, Immunity (2023), https://doi.org/10.1016/j.immuni.2023.04.013

cell infiltrates and resident glial cell populations are consequential to MS[3]; however, the communication axes that mediate peripheral-central crosstalk in the diseased CNS remain ill-defined, despite their therapeutic potential.[2,4]

Interleukin-3 (IL-3) is a multifaceted cytokine and growth factor implicated in inflammatory and autoimmune diseases.[5,6] A member of the colony-stimulating factor family, IL-3 has been linked to immune disorders including sepsis,[7] atherosclerosis,[8] lupus nephritis,[9] and arthritis.[10] These studies have mostly focused on IL-3's function as a hematopoietic growth factor and an endocrine stimulant of monocytosis, while IL-3's impact beyond its action on BM and splenic hematopoietic stem and progenitor cells is less clear. IL-3's contributions to brain health and disease have remained largely unknown. Recently, we have demonstrated a fundamental, protective role for IL-3 in Alzheimer disease (AD) where it instigates clearance of β-amyloid (Aβ) and tau by microglia.[11] Yet the function of IL-3 in other neuroinflammatory contexts, including CNS autoimmunity, MS, and its murine model experimental autoimmune encephalomyelitis (EAE), has remained undefined. While some reports suggest IL-3 may play a role in demyelinating animal models, these studies have employed non-specific tools, producing contradictory results,[12,13] or used artificial overexpression systems.[14–16] For example, the consequential cell populations that generate the cytokine or functionally respond to it in the inflamed CNS remain unknown, and this axis's role in the CNS of humans with MS is uncertain. The communication systems among resident glial cells and infiltrating immune cells in the inflamed CNS are unresolved, despite being an emerging node for therapeutic intervention.[17] Therefore, there is a clear need to examine, define, and resolve the IL-3:IL-3Rα dyad in mice and humans, using contemporary tools to advance our fundamental understanding of the disease and therapeutic applications.

Here, we report that, in human MS and its murine model, CNS-resident astrocytes and infiltrating $CD44^{hi}CD4^{+}$ T cells produce IL-3 that instigates a migratory and chemotactic program by IL-3Rα-expressing CNS-resident microglia and peripherally derived myeloid cells that perpetuates immune cell recruitment, CNS inflammation, and clinical and pathological severity. In humans, cerebrospinal fluid (CSF) IL-3 amount predicted clinical MS diagnosis and severity. In mice, deletion of *Il3* or *Il3ra* globally or specifically from their relevant cellular sources improved EAE and neural demyelination and restricted immune cell recruitment to the CNS by dampening myeloid-derived chemotactic cues. In humans, regionally defined single-nuclei RNA sequencing (snRNA-seq) of white and gray matter (WM and GM) tissue from control individuals and MS patients and pathologic plaque tissue of MS patients demonstrated that *IL3RA*-expressing myeloid cells represent a unique subset that accumulates in MS plaques and is endowed with immune cell migration and chemotactic properties. Further, plaque myeloid cell *IL3RA* expression and CSF IL-3 amount associated with immune cell recruitment to the CNS of MS patients. These findings define IL-3 as a critical mediator of central-peripheral immune crosstalk and a regulator of CNS myeloid cell programming and neuroinflammation in MS.

RESULTS

IL-3 associates with human RRMS and exacerbates spinal cord inflammation, demyelination, and clinical severity in EAE

Given our limited knowledge of IL-3 in neuroinflammation, we tested if IL-3 is relevant in human MS. To do so, we measured the cytokine in the CSF, a disease-relevant compartment that sensitively reflects immunogenic processes occurring in the CNS,[18,19] of 36 patients with clinically diagnosed relapsing remitting MS (RRMS) and 35 age-matched unaffected controls. We found that, relative to control donors, RRMS patients had elevated IL-3 in their CSF (Figure 1A). In controls and RRMS patients, CSF IL-3 amount did not depend on sex (Figure S1A), and among RRMS patients, IL-3 did not depend on whether CSF was collected during phases of remission or relapse (Figure S1B). We then analyzed a separate cohort of patients with clinically isolated syndrome (CIS) who experienced one symptomatic episode of MS and observed that CSF IL-3 was increased in patients who converted to fully diagnosed MS (according to the Poser criteria), compared with individuals who did not convert to a clinical MS diagnosis (non-converters) over a >2-year follow-up (Figure 1A). Again, CSF IL-3 was not influenced by sex among converters and non-converters (Figure S1C). Together, these findings put forth a role for IL-3 in the CNS of humans with MS.

To begin mechanistically exploring the function of IL-3 during MS-like neuroinflammation and neurodegeneration, we adopted the murine model of MS, EAE, in which mice are injected with myelin oligodendrocyte glycoprotein suspended in complete Freund's adjuvant ($MOG_{35–55}$/CFA) and pertussis toxin (PTX) causing spinal cord (SC) inflammation, impaired neuromuscular and sensory function, demyelination, and paralysis.[20] First, we measured *Il3* expression in relevant organs of naive and EAE mice at peak disease. While EAE did not change *Il3* expression in the lymph nodes or spleen (Figure S1D), *Il3* was significantly higher in the SC of EAE mice relative to healthy controls (Figure 1B). To test if IL-3 has a functional role in EAE, we induced EAE in wild-type (WT) and IL-3-deficient ($Il3^{-/-}$) mice and monitored clinical disease development over 21 days post immunization (dpi). Clinical assessment revealed that despite similar disease onset, $Il3^{-/-}$ mice had improved clinical scores and were profoundly protected from disease severity and paralysis (Figure 1C). In MS and EAE, paralysis caused by axonal damage and neuro-muscular degeneration is attributed to neuronal demyelination.[1,21] To determine IL-3's impact on myelination, we stained SC sections of diseased WT and $Il3^{-/-}$ mice with Luxol fast blue and quantified neuropil and demyelinated areas (Figure 1D). This analysis uncovered substantially reduced demyelination throughout the SC of $Il3^{-/-}$ mice affecting the cervical, thoracic, lumbar, and sacral regions (Figure 1D). These data suggest that IL-3 contributes to demyelination and worsens neuronal integrity, aggravating EAE severity.

We next tested the immunogenic and encephalitogenic functions of IL-3 in EAE. Improved clinical outcomes and reduced disease severity in $Il3^{-/-}$ mice may be due to either alterations in peripheral immune priming in medullary organs or changes in the effector organ, the CNS, which diminish immune cell infiltrates and neuroinflammation. To test the former, we first

Please cite this article in press as: Kiss et al., Interleukin-3 coordinates glial-peripheral immune crosstalk to incite multiple sclerosis, Immunity (2023), https://doi.org/10.1016/j.immunu.2023.04.013

CellPress

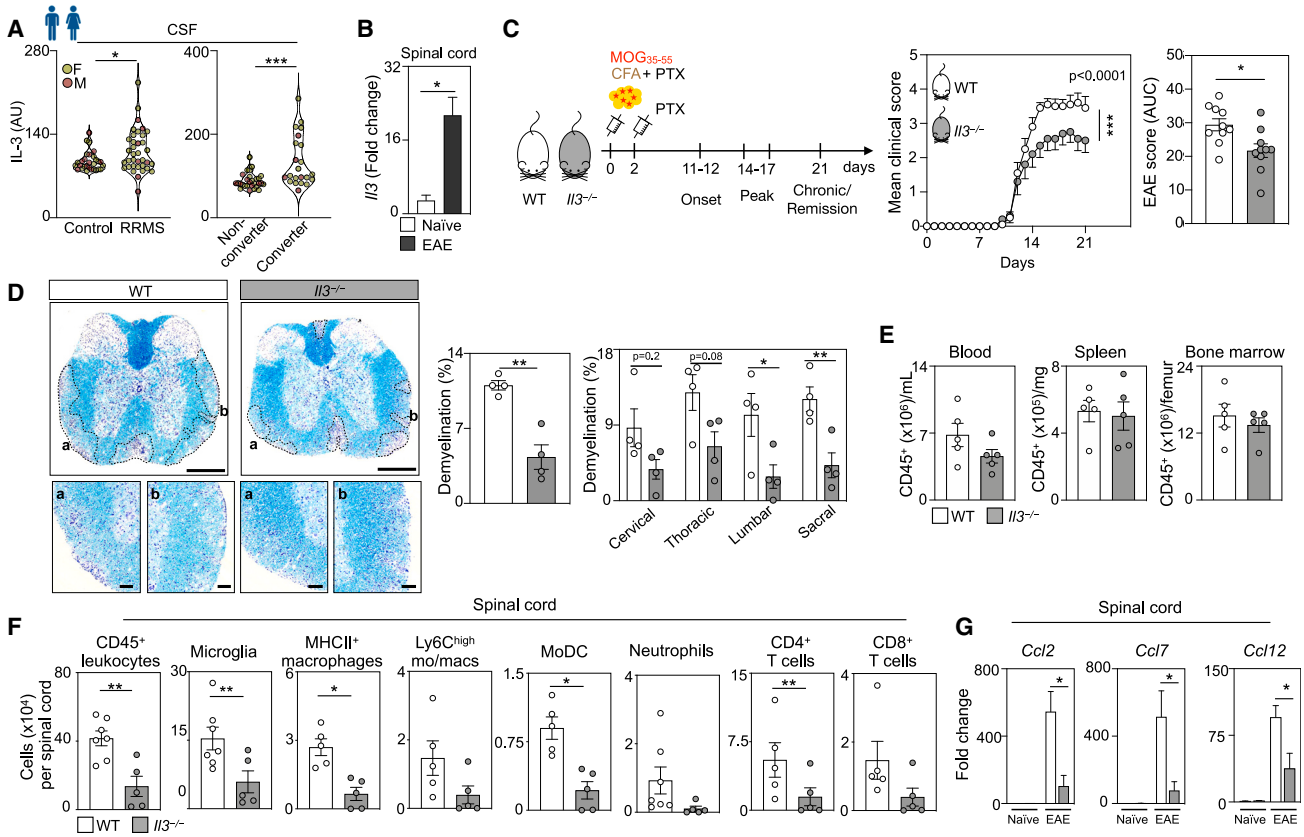

Figure 1. Interleukin-3 associates with human RRMS and exacerbates spinal cord inflammation, demyelination, and EAE

(A) Left: IL-3 amount in the CSF of male and female unaffected control subjects and patients with RRMS. Right: baseline CSF IL-3 amount in male and female non-converters and patients who converted to MS diagnosis over a 2-year follow-up (n = 29 controls, 36 RRMS patients, 28 non-converters, 22 converters; Mann-Whitney U tests).

(B) Il3 gene expression in the spinal cord in WT EAE mice at disease peak and naive mice (n = 4–5 mice/group; Mann-Whitney U test).

(C) Schematic diagram of the experimental design. EAE was induced in WT and *Il3*$^{-/-}$ mice by administering myelin oligodendrocyte glycoprotein ($MOG_{35–55}$) peptide emulsified in complete CFA by subcutaneous injection on day 0 and PTX by intraperitoneal injections on days 0 and 2. Mean clinical disease scores and corresponding AUC analysis of WT and *Il3*$^{-/-}$ mice over the course of 21 dpi (n = 10 mice/group; two-way ANOVA and Mann-Whitney U test).

(D) Representative histological sections of 4 mice per group and quantification of demyelinated area in diseased spinal cords from WT and *Il3*$^{-/-}$ mice stained for myelin by luxol fast blue and counterstained with cresyl echt violet solution at disease peak. Scale bars represent 500 μm for overview images and 100 μm for the inset images (n = 4 mice/group; two-way ANOVA and Mann-Whitney U test).

(E) Quantification of CD45$^+$ leukocyte numbers in the blood, spleen, and bone marrow of WT and *Il3*$^{-/-}$ mice at the disease peak (n = 5 mice/group).

(F) Quantification of leukocyte subsets in the spinal cord of WT and *Il3*$^{-/-}$ mice at the disease peak (n = 5–7 mice/group; Mann-Whitney U tests).

(G) qPCR analysis of chemokine transcript expression in the spinal cord of healthy and EAE WT and *Il3*$^{-/-}$ mice (n = 4–5 mice/group; one-way ANOVA).

Mean ± SEM, *p < 0.05, **p < 0.01, and ***p < 0.001.

CSF, cerebrospinal fluid; RRMS, relapsing remitting multiple sclerosis; AUs, arbitrary units; IL-3, interleukin-3; WT, wild type; EAE, experimental autoimmune encephalomyelitis; CFA, Freund's adjuvant; PTX, pertussis toxin; MOG, myelin oligodendrocyte glycoprotein; AUC, area under the curve; dpi, days post immunization.

See also Figures S1 and S2.

enumerated peripheral immune cells and found equivalent numbers of T cells, B cells, neutrophils, and monocytes in the blood, spleen, and BM of diseased WT and *Il3*$^{-/-}$ mice (Figures 1E, S1E, and S1F). Pursuing immune priming more specifically, we measured CD4$^+$ T_H cell abundance and proliferation in the spleen and lymph nodes and found that *Il3* deletion did not influence these parameters (Figures S2A and S2B). We next evaluated pro-inflammatory IFN-γ$^+$, IL-17A$^+$, IFN-γ$^+$IL-17A$^+$, and GM-CSF$^+$ T_H cell subsets in the spleen and lymph nodes and again did not find alterations in *Il3*$^{-/-}$ mice (Figures S2C and S2D). Further, we also observed that IL-3 did not change the amount of resident, migratory, and monocyte-derived dendritic cells (MoDCs) in spleen and lymph nodes, nor did it influence their expression of the costimulatory molecules MHCII, CD80, CD86, and OX40L (Figures S2E–S2H). To expand on this analysis, we performed *ex vivo* splenocyte recall response assays to increasing concentrations of $MOG_{35–55}$ and found that IL-3 deficiency did not influence the capacity of T cells to proliferate or produce cytokines (Figures S2I and S2J). All together, these results show IL-3 is dispensable for peripheral priming of myeloid-reactive CD4$^+$ T cells in EAE.

Please cite this article in press as: Kiss et al., Interleukin-3 coordinates glial-peripheral immune crosstalk to incite multiple sclerosis, Immunity (2023), https://doi.org/10.1016/j.immuni.2023.04.013

We then turned our attention to the effector organ. EAE and MS are characterized by recruitment of peripheral immune cells to the CNS that contribute to an inflammatory milieu and aggravate disease severity.[22,23] We found that IL-3 deficiency significantly reduced the number of CD45$^+$ leukocytes in the SC at peak disease (Figure 1F). Flow cytometric analysis of the SC revealed that *Il3*$^{-/-}$ mice had reductions in important EAE-relevant immune cell populations, including microglia, and peripherally derived MHCII$^+$ macrophages, MoDCs, and CD4$^+$ T cells (Figures 1F and S1G), proposing that IL-3 plays a role in immune cell recruitment to the CNS. To assess the impact of IL-3 on immune cell recruitment more carefully, we measured key chemoattractants. In WT animals, EAE robustly augmented the expression of *Ccl2*, *Ccl7*, and *Ccl12* in the SC (Figure 1G). Meanwhile, in *Il3*$^{-/-}$ mice, the generation of this chemotaxis program was significantly blunted (Figure 1G). These findings suggest IL-3 plays a pathogenic role in the SC by driving local inflammation and immune cell recruitment during the effector phase of EAE, leading to paralysis and disability without overt influence on peripheral leukocyte priming, abundance, or function.

Astrocytic IL-3 potentiates EAE

Having established a pathogenic role for IL-3 in EAE, we next sought the relevant cell types that generate the cytokine. Flow cytometric analysis of WT EAE mice suggested that both hematopoietic and non-hematopoietic cells produce IL-3 in the SC (Figure 2A). Among CD45$^+$ hematopoietic cells, we identified CD44^{hi}CD4$^+$ T cells as sources of IL-3, and among non-hematopoietic cells, we found that GFAP$^+$ACSA-2$^+$ astrocytes abundantly produce IL-3 (Figure 2A). Robust *Il3* transcript expression was confirmed in CD44^{hi}CD4$^+$ T cells and astrocytes sorted from the diseased SC (Figure S3A). To further verify IL-3 generation by astrocytes, we performed immunofluorescent imaging and found that IL-3-producing cells overlapped with glial fibrillary acidic protein (GFAP), an astrocyte marker, in the diseased SC (Figures 2B, S3B, and S3C). Quantification of our flow cytometric data revealed that CD4$^+$ T cells and astrocytes produced IL-3 in approximately equivalent proportions and that these populations accounted for nearly all the IL-3 generated in the SC of EAE mice (Figure 2C). Critically, these findings identify two local sources of IL-3 in the SC; however, their relative contributions to neuroinflammation and disease severity remained unknown.

To delineate the relevance of these disparate cellular sources of IL-3, we first sought to decipher the contribution of astrocytic IL-3 to CNS inflammation and EAE. Quantification of astrocyte IL-3 production in healthy animals and at various stages of EAE suggested that IL-3$^+$ astrocytes comprise ~5% of the astrocytic pool in the SC (Figure 2D) and that the abundance of IL-3$^+$ astrocytes, and their relative generation of the cytokine, remained unchanged in EAE animals at 3, 14, and 28 dpi (Figure 2E). In agreement, imaging of the EAE SC did not reveal a difference in the abundance of IL-3$^+$GFAP$^+$ astrocytes in demyelinated plaques relative to adjacent unaffected tissue (Figure S3D). To test the specific contribution of astrocyte-sourced IL-3 to EAE, we crossed *Il3*$^{GFPfl/fl}$ mice with *Aldh1l1cre*^{Ert2} mice to generate tamoxifen-inducible astrocyte-specific IL-3 deficient animals (*Il3*$^{GFPfl/fl}$*Aldh1l1cre*^{Ert2}). We then used a tamoxifen injection strategy to delete astrocytic IL-3 in adult mice prior to EAE induction (Figure S3E).[11] Tamoxifen-injected *Il3*$^{GFPfl/fl}$*Aldh1l1cre*^{Ert2} EAE mice had robust deletion of astrocytic, but not T cell, IL-3 and reduced total IL-3 amount in SC homogenate but not in the plasma (Figures S3F–S3H). Compared with tamoxifen-injected *Il3*$^{GFPfl/fl}$ littermate controls and beginning at early disease stages, astrocyte-specific *Il3* deletion significantly improved clinical disease score and ameliorated paralysis (Figure 2F), a phenotype we observed in both male and female mice (Figure S3I). Moreover, relative to control *Il3*$^{GFPfl/fl}$ mice, diseased *Il3*$^{GFPfl/fl}$ *Aldh1l1cre*^{Ert2} mice had fewer CD4$^+$ T cell infiltrates in the SC (Figure 2G), lower expression of the chemokines *Ccl2* and *Ccl5*, and a tendency toward reduced *Ccl7* in the SC (Figure 2H). Together, these data reveal that astrocytic IL-3 plays a pathogenic role in CNS inflammation in EAE.

IL-3$^+$CD44^{hi}CD4$^+$ T$_H$ cells worsen EAE and spinal cord inflammation

Given that MS is a T cell-mediated CNS autoimmune disease driven by encephalitogenic CD4$^+$ T cells and that we identified CD44^{hi}CD4$^+$ T cells as hematopoietic producers of IL-3, we next assessed whether IL-3 generated by these cells impacts EAE. First, we monitored the kinetics and phenotype of IL-3$^+$ CD44^{hi}CD4$^+$ T cells in the periphery and CNS during EAE. Using our dual IL-3-GFP reporter and floxed mice (*Il3*$^{GFPfl/fl}$), we quantified GFP$^+$CD44^{hi}CD4$^+$ T cells in peripheral tissues and the SC at 8,12,16, and 22 days post EAE induction. The number of IL3^{GFP+}CD44^{hi}CD4$^+$ T cells peaked at 8 dpi in the blood, BM, spleen, and lymph nodes, revealing the generation and systemic mobilization of these cells during early disease stages (Figure 3A). In the SC, we observed notable recruitment of IL3^{GFP+}CD44^{hi}CD4$^+$ T cells, peaking at day 12 and remaining elevated throughout later disease time points (Figure 3A). In the SC, IL3^{GFP+}CD44^{hi}CD4$^+$ T cells expressed the homing molecule CD62L (Figure S3J), suggesting that they were antigen-experienced effectors, and their abundance was heightened at all grades of clinical severity (Figure S3K). We next tested IL-3 production by specific T helper (T$_H$) cell lineages in the diseased SC and found that the cytokine is broadly generated by T$_H$1, T$_H$17, IL-17A$^+$IFN-γ^+, and GM-CSF$^+$ cells (Figure 3B), indicating that IL-3 is produced by many T$_H$ cell types in the CNS. These findings demonstrate the systemic mobilization of IL-3 producing effector T cells and their recruitment to the CNS during EAE.

We next explored whether IL-3 serves as a crucial pathogenic T cell-derived factor in EAE. To generate T cell-specific IL-3-deficient mice, we crossed *Il3*$^{GFPfl/fl}$ with *Cd4cre* mice and subjected the resulting *Il3*$^{GFPfl/fl}$*Cd4cre* animals, along with *Il3*$^{GFPfl/fl}$ littermate controls, to EAE. First, we confirmed *Il3* transcript deletion in T cells, but not in astrocytes, sorted from the SC of diseased *Il3*$^{GFPfl/fl}$*Cd4cre* mice (Figure S3L). Moreover, flow cytometry demonstrated a robust reduction in IL-3 production by T cells in the SC, spleen, and lymph node of diseased *Il3*$^{GFPfl/fl}$*Cd4cre* mice (Figure S3M). Together, this resulted in lower IL-3 amount in SC homogenate but not in plasma of *Il3*$^{GFPfl/fl}$*Cd4cre* mice (Figure S3N). After inducing EAE in *Il3*$^{GFPfl/fl}$ and *Il3*$^{GFPfl/fl}$*Cd4cre* mice, we found that despite equivalent disease onset, T cell-specific *Il3* deletion protected against EAE development, clinical symptoms, and paralysis (Figure 3C). Importantly, we found that both male and female *Il3*$^{GFPfl/fl}$*Cd4cre* mice were protected from disease (Figure S3O). Flow cytometric enumeration analysis of the SC revealed a blunting of immune cell infiltrates in

Please cite this article in press as: Kiss et al., Interleukin-3 coordinates glial-peripheral immune crosstalk to incite multiple sclerosis, Immunity (2023), https://doi.org/10.1016/j.immuni.2023.04.013

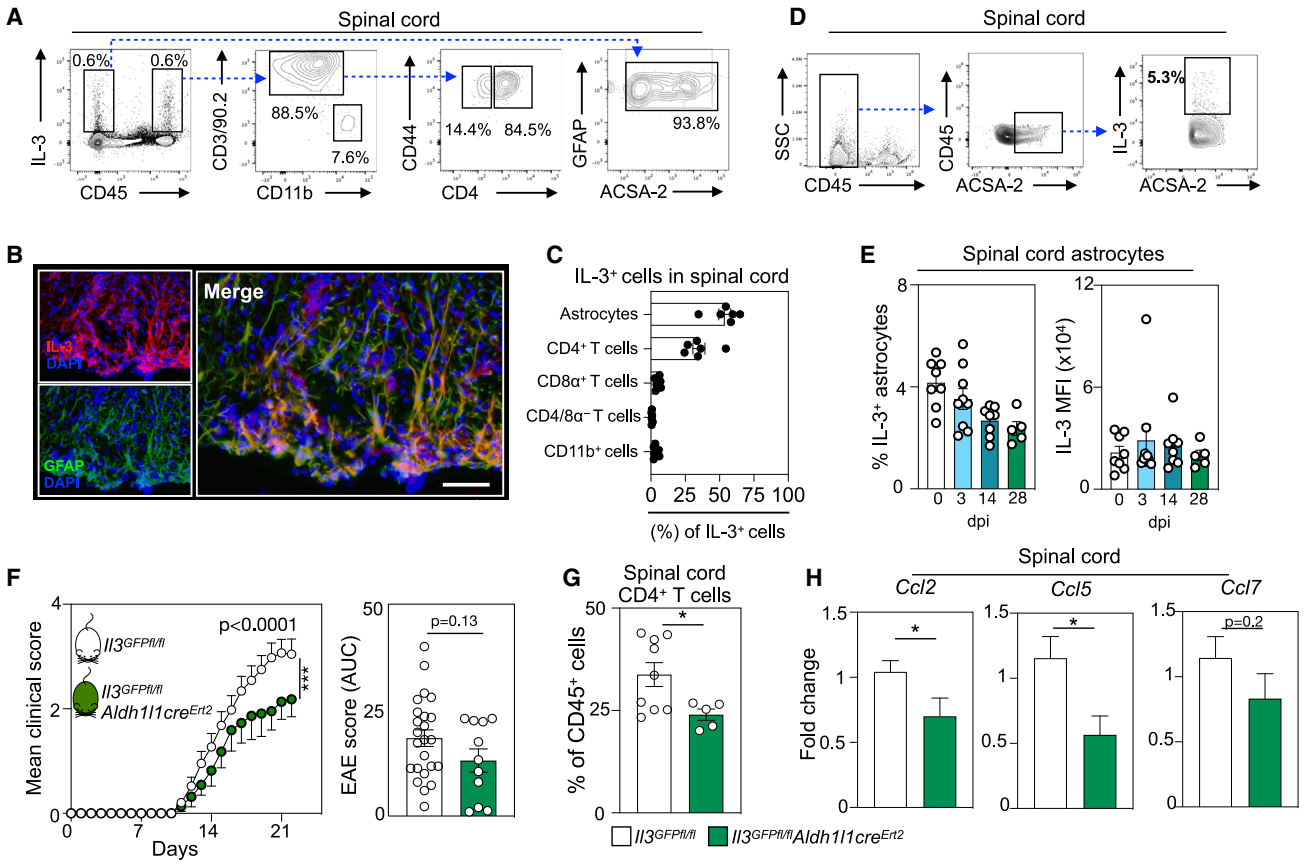

Figure 2. CD44^{hi} CD4^{+} T cells and astrocytes generate IL-3 in the CNS and astrocytic IL-3 potentiates EAE

(A) Flow cytometric analysis of IL-3-producing cells in the spinal cords of WT mice at the peak of EAE.

(B) Representative immunofluorescent images of the spinal cord of 4 mice showing IL-3 co-localization with the astrocyte marker GFAP in WT EAE mice at peak disease. Scale bar represents 50 μm.

(C) Flow cytometric quantification of IL-3-producing cells in the spinal cord of WT EAE mice at disease peak (n = 6 mice).

(D) Flow cytometric gating strategy identifying IL-3-producing astrocytes in the spinal cord.

(E) Quantification of IL-3 production by spinal cord astrocytes during the course of EAE development (n = 5–9 mice/group).

(F) Mean clinical disease scores and corresponding AUC analysis of *Il3*$^{GFPfl/fl}$ and *Il3*$^{GFPfl/fl}$*Aldh1l1cre*^{Ert2} male and female mice injected with tamoxifen and induced with EAE (n = 11–24 mice/group; two-way ANOVA and Mann-Whitney U test).

(G) Flow cytometric quantification of infiltrating CD4^{+} T cells in the spinal cord of *Il3*$^{GFPfl/fl}$ and *Il3*$^{GFPfl/fl}$*Aldh1l1cre*^{Ert2} mice injected with tamoxifen and induced with EAE (n = 5–9 mice/group; Mann-Whitney U test).

(H) qPCR analysis of chemokine transcript expression in the spinal cord of *Il3*$^{GFPfl/fl}$ and *Il3*$^{GFPfl/fl}$*Aldh1l1cre*^{Ert2} mice injected with tamoxifen and exposed to EAE (n = 9–13 mice/group; Mann-Whitney U tests).

Mean ± SEM, *p < 0.05, **p < 0.01, and ***p < 0.001.

WT, wild type; EAE, experimental autoimmune encephalomyelitis; GFAP, glial fibrillary acidic protein; DAPI, 4′,6-diamidino-2-phenylindole; AUC, area under the curve; dpi, days post immunization; MFI, mean fluorescence intensity.

See also Figure S3.

Il3$^{GFPfl/fl}$*Cd4cre* mice at disease peak (Figure 3D). Further, gene expression analysis revealed reduced *Ccl5* and a tendency toward reduced *Ccl2* and *Ccl7* in the SC of *Il3*$^{GFPfl/fl}$*Cd4cre* mice (Figure 3E). Together, these data identify CD44^{hi}CD4^{+} T_H cells as pathogenic hematopoietic sources of IL-3 that potentiate SC inflammation and worsen EAE severity.

CNS myeloid cells express IL-3Rα and exacerbate spinal cord inflammation, demyelination, and chemokine generation

Having identified T cells and astrocytes as relevant pathogenic sources of IL-3 in EAE, we next sought the cells that respond to the cytokine. IL-3Rα (also known as CD123) is IL-3's specific receptor, and immunofluorescent imaging suggested that CD11b^{+} myeloid cells express IL-3Rα in the diseased SC (Figure 4A). To explore this, we adopted a stringent flow cytometry gating strategy to identify the specific myeloid cells that express IL-3Rα in the SC (Figure 4B). We found that during EAE resident microglia augmented IL-3Rα becoming responsive to IL-3 (Figure S4A) and that among myeloid populations infiltrating the SC, MHCII^{+} macrophages, Ly6C^{hi} monocytes and macrophages, and MoDCs are major expressors of IL-3Rα (Figure 4C). We confirmed these data at the transcriptional level by measuring *Il3ra* mRNA expression in myeloid cells sorted from

Please cite this article in press as: Kiss et al., Interleukin-3 coordinates glial-peripheral immune crosstalk to incite multiple sclerosis, Immunity (2023), https://doi.org/10.1016/j.immuni.2023.04.013

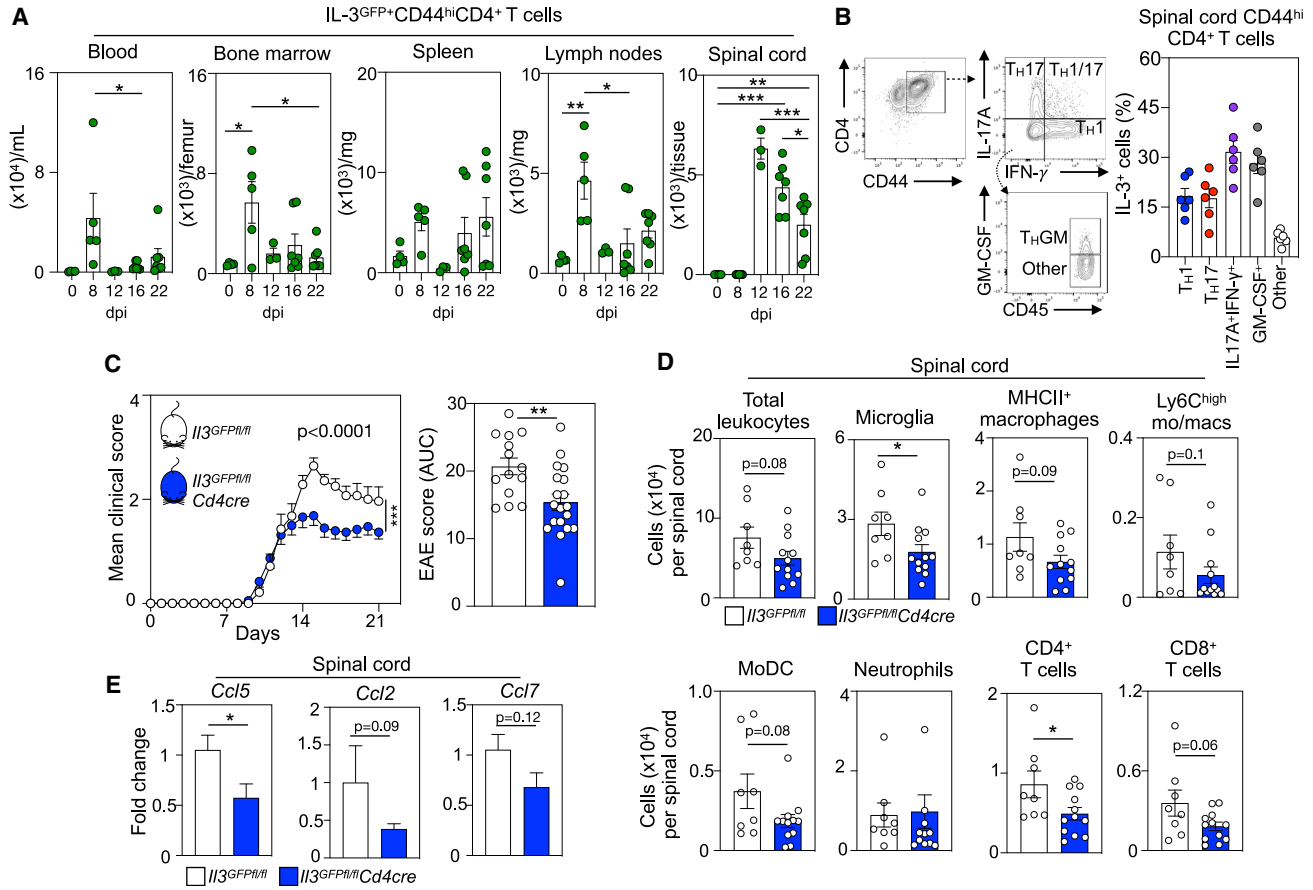

Figure 3. IL-3 production by CD4⁺ CD44^{hi} effector T_H cells promotes EAE development

(A) Flow cytometric quantification of IL-3^{GFP+}CD44^{hi}CD4$^+$ T cells in the blood, bone marrow, spleen, lymph nodes, and spinal cord throughout the course of EAE (n = 3–7 mice/ group; two-way ANOVA).

(B) Flow cytometric analysis of IL-3$^+$ cell frequency among T_H1 (IFN-γ^+), T_H17(IL-17A$^+$), IL-17A$^+$IFN-γ^+ (IFN-γ^+ IL-17A$^+$), GM-CSF$^+$ (GM-CSF$^+$ IFN-γ^+ IL-17A$^-$), and other (GM-CSF$^-$ IFN-γ^- IL-17A$^-$) CD44^{hi} CD4$^+$ T_H cells in the spinal cord at the peak of EAE (n = 6 mice).

(C) Mean clinical scores and corresponding AUC analysis of *Il3*$^{GFPfl/fl}$ and *Il3*$^{GFPfl/fl}$*Cd4cre* male and female mice exposed to EAE (n = 14–19 mice/group; two-way ANOVA and Mann-Whitney U test).

(D) Quantification of leukocyte subsets in the spinal cord of *Il3*$^{GFPfl/fl}$ and *Il3*$^{GFPfl/fl}$*Cd4cre* mice at the disease peak by flow cytometry (n = 8–12 mice/group; Mann-Whitney U tests).

(E) qPCR analysis of chemokine transcript expression in the spinal cord of *Il3*$^{GFPfl/fl}$ and *Il3*$^{GFPfl/fl}$*Cd4cre* mice subjected to EAE (n = 6–12 mice/group; Mann-Whitney U tests).

Mean ± SEM, *p < 0.05, **p < 0.01, and ***p < 0.001.

EAE, experimental autoimmune encephalomyelitis; AUC, area under the curve; dpi, days post immunization.

See also Figure S3.

the diseased SC (Figure 4D). The abundance of IL-3Rα-expressing microglia, MHCII$^+$ macrophages, Ly6C^{hi} monocytes and macrophages, and MoDCs in the SC increased in EAE and correlated with clinical disease severity (Figure S4B).

To test for a consequential role of IL-3Rα in EAE, we designed a CRISPR-Cas9 nuclease-based editing strategy with dual guide RNAs (gRNAs) to delete exons 2–11 of the endogenous *Il3ra* sequence, thus generating *Il3ra*$^{-/-}$ mice (Figure S4C). First, we confirmed successful deletion of IL-3Rα (Figures S4D and S4E), and then we subjected WT and *Il3ra*$^{-/-}$ mice to EAE and monitored clinical disease severity. We found that *Il3ra* deletion significantly improved clinical symptoms and paralysis (Figure 4E). Luxol fast blue staining of SC sections (Figure 4F) revealed profoundly reduced demyelination in the cervical, thoracic, and lumbar regions of *Il3ra*$^{-/-}$ mice (Figure 4G). We then measured immune cell infiltrates to the SC of WT and *Il3ra*$^{-/-}$ mice and found that *Il3ra* deletion robustly limited total CD45$^+$ leukocytes, MHCII$^+$ macrophages, and MoDCs, while neutrophils and CD4$^+$ T cells tended to decrease (Figure 4H). Together, these observations confirm that IL-3-sensing myeloid cells play an essential and detrimental role in neuroinflammation and EAE.

Next, we aimed to better understand how IL-3 influences CNS myeloid cell programming and function. First, we sorted CD45$^+$CD11b$^+$ monocytes from the BM of WT mice and stimulated them with recombinant IL-3 (rIL-3) *ex vivo*. We found that rIL-3 incited expression of genes indicative of differentiation and maturation into myeloid antigen-presenting cells (APCs),

Please cite this article in press as: Kiss et al., Interleukin-3 coordinates glial-peripheral immune crosstalk to incite multiple sclerosis, Immunity (2023), https://doi.org/10.1016/j.immunu.2023.04.013

CellPress

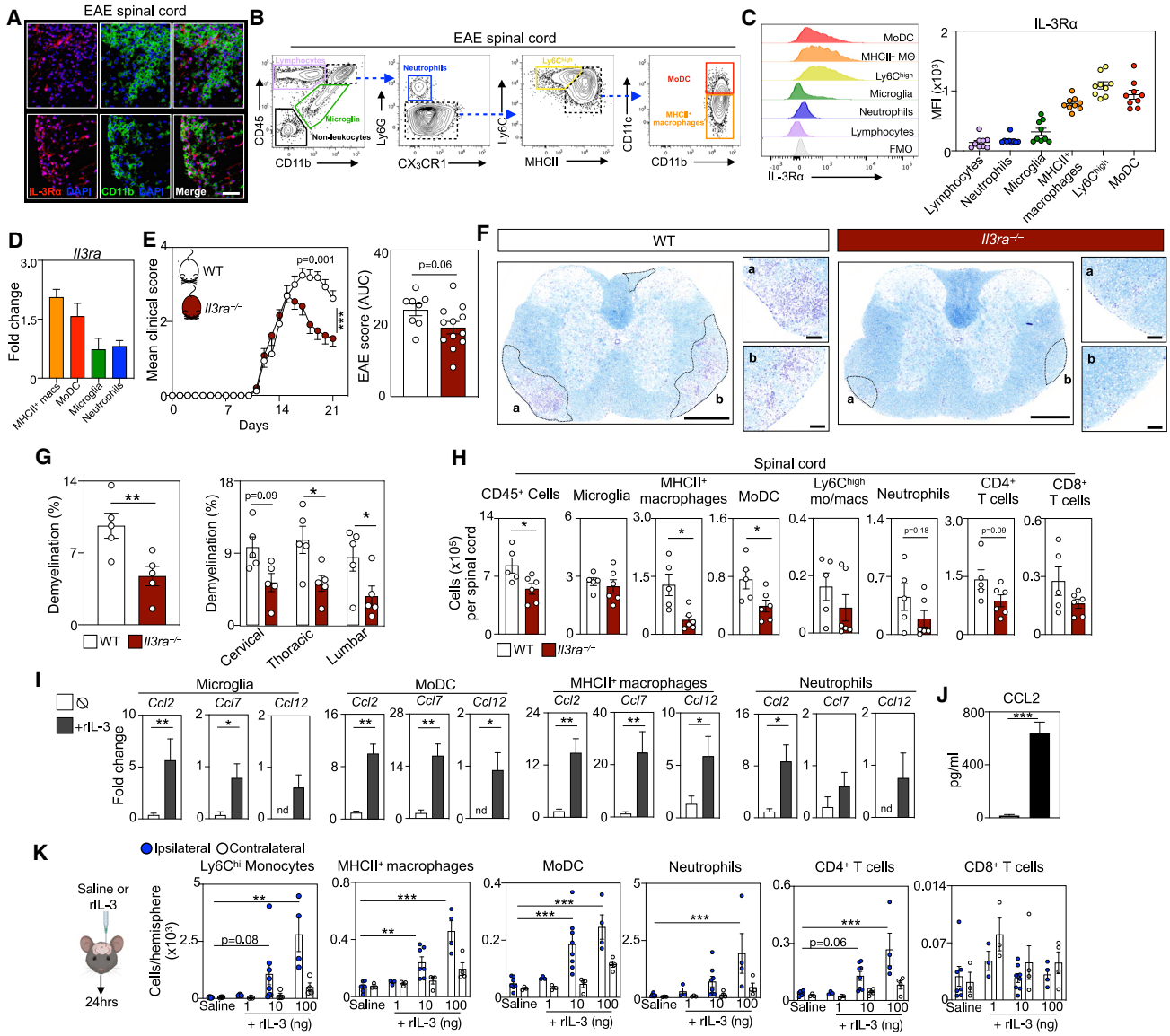

Figure 4. Spinal cord myeloid cells express IL-3Rα and aggravate EAE by instigating immune cell recruitment to the CNS

(A) Representative immunofluorescent images of IL-3Rα (CD123) and CD11b on spinal cord sections of 4 WT EAE mice at disease peak. Scale bar is 100 μm.

(B) Flow plots showing the cell gating strategy for leukocytes and non-leukocytes in the spinal cords of WT EAE mice at peak disease.

(C) Flow cytometric analysis and quantification of IL-3Rα expression by spinal cord cells at peak disease (n = 9 mice).

(D) qPCR analysis of *Il3ra* expression by myeloid cells sorted from the spinal cord at disease peak (n = 4–5 mice).

(E) Mean clinical score and corresponding AUC analysis of WT and *Il3ra*$^{-/-}$ mice during EAE (n = 8–12 mice/group; two-way ANOVA and Mann-Whitney U test).

(F) Representative histological sections of demyelination in diseased spinal cords from 5 WT and 5 *Il3ra*$^{-/-}$ mice stained for myelin by luxol fast blue and counterstained with cresyl echt violet solution at disease peak. Scale bars represent 500 μm for overview images and 100 μm for the inset images.

(G) Quantification of demyelination area in diseased spinal cords from WT and *Il3ra*$^{-/-}$ mice (n = 5 mice/group; two-way ANOVA and Mann-Whitney U test).

(H) Flow cytometric analysis of spinal cord CD45^{+} leukocyte subsets in WT and *Il3ra*$^{-/-}$ mice at peak disease (n = 5–6 mice/group; Mann-Whitney U tests).

(I) Transcript expression analysis in myeloid cells sorted from the spinal cord of WT EAE mice at the peak of disease and stimulated with rIL-3 (n = 5 group; Mann-Whitney U tests).

(J) Measurement of CCL2 in the media of monocyte cultures exposed to rIL-3 (n = 5 group; Mann-Whitney U test).

(K) Enumeration of immune cells in the brain of mice 24 h after stereotactic injection of 0, 1, 10, or 100 ng rIL-3 (n = 3–8 mice/group; one-way ANOVA).

Mean ± SEM, *p < 0.05, **p < 0.01, and ***p < 0.001.

WT, wild type; EAE, experimental autoimmune encephalomyelitis; MFI, mean fluorescence intensity; rIL-3, recombinant interleukin-3.

See also Figure S4.

Please cite this article in press as: Kiss et al., Interleukin-3 coordinates glial-peripheral immune crosstalk to incite multiple sclerosis, Immunity (2023), https://doi.org/10.1016/j.immuni.2023.04.013

including *Arg1*, *Mrc1*, *Zbtb46*, *CD209*, and *Mertk*, while reducing the monocytic genes *Ly6c2* and *C5ar1* (Figure S4F). Likewise, flow cytometry analysis showed that IL-3 signaled via IL-3Rα to promote monocyte differentiation into MHCII$^+$CD86$^+$CD80$^+$ CD11c$^+$Ly6C$^-$ APCs (Figures S4G and S4H). Given our data on IL-3's role in immune cell abundance and recruitment to the CNS, we hypothesized that IL-3 stimulates the generation of chemotactic and migratory cues by IL-3Rα$^+$ myeloid cells in the SC. To test this, we sorted microglia, MoDCs, MHCII$^+$ macrophages, and neutrophils from the SC of EAE mice and stimulated them *ex vivo* with rIL-3, which robustly increased the expression of the chemokines *Ccl2*, *Ccl7*, and *Ccl12* (Figure 4I). rIL-3 treatment also raised CCL2 protein abundance in the culture media (Figure 4J). To expand on this, we polarized splenic T cells into T_H1, $T_H17(\beta)$, or $T_H17(23)$ subsets, co-cultured them with WT or *Il3ra*$^{-/-}$ BM monocytes, and found that IL-3Rα deficiency decreased T cell-induced CCL2 generation (Figure S4I). To specifically test IL-3's ability to stimulate immune cell recruitment to the CNS *in vivo*, we stereotactically injected mice with saline or 1, 10, or 100 ng of rIL-3 into their striata (Figure 4K). Stereotactic delivery of rIL-3 robustly induced Ly6C^{hi} monocyte, MHCII$^+$ macrophage, MoDC, neutrophil, and CD4$^+$ T cell—but not CD8$^+$ T cell or B cell—recruitment to the CNS in a dose-dependent manner (Figures 4K and S4J). Taken together, these findings demonstrate that IL-3 promotes the differentiation of monocyte-derived APCs and the generation of chemotactic cues by resident and recruited IL-3Rα$^+$ myeloid cells, which stimulate further infiltration of relevant immune cells to the CNS, thereby exacerbating neuroinflammation and EAE.

IL-3:IL-3RA promotes accrual of migratory and chemotactic myeloid cell subsets in human MS plaques

Having established a role for the IL-3:IL-3Rα dyad in a murine model of MS, we returned our attention to humans. For an in-depth regional analysis of cell dynamics in the CNS of MS patients, we performed snRNA-seq on dissected regions of human brain tissue. We separately sequenced WM and GM tissue from six unaffected control subjects and six MS patients along with demyelinated plaques from the MS patients (Figure 5A). Across all tissues and diagnoses, a total of 77,490 nuclei were sequenced that clustered into all major CNS cell types including myeloid cells, T cells, astrocytes, oligodendrocytes, oligodendrocyte progenitor cells (OPCs), endothelial cells (ECs), vascular leptomeningeal cells (VLMCs), and neurons (multiple clusters of GABAergic and glutamatergic neurons) (Figure 5B). First, we quantified cell abundance across tissue regions in control subjects and MS patients. As expected, we found more neurons in GM relative to WM and more oligodendrocytes in WM (Figure S5A). We then assessed the cellular composition of MS plaques, which typically evolve in WM, and found few neurons and oligodendrocytes (Figure S5A) but more astrocytes, T cells, and myeloid cells relative to other regions and tissue from control subjects (Figure 5C), reflective of the inflammatory and immunogenic milieu of MS plaques in the human CNS. To better understand how CNS myeloid cells are reprogrammed in plaques, we compared myeloid cells isolated from plaques with those from adjacent unaffected WM tissue in MS patients. Transcriptional analysis revealed that myeloid cells in MS plaques profoundly induced pathways associated with immune cell migration, recruitment, and activation (Figure 5D, left) and upregulated chemotactic genes including *CCL2*, *CCL3*, *CCL4*, *CCL5*, *CXCL2*, *CXCL12*, *CXCL13*, and *CXCL16* and their associated receptors *CCR1*, *CCR2*, *CCR5*, *CXCR4*, and *CX3CR1* (Figure 5D, right). These data affirm the inflammatory nature of myeloid cells in the MS plaque microenvironment and demonstrate their activation of chemotactic and immune cell recruitment processes.

We next evaluated *IL3RA* expression across all CNS cell types, tissular regions, and diagnoses. In unaffected subjects and MS patients, we found that *IL3RA* was expressed widely by all CNS cells in WM and GM and in the plaques of MS patients (Figures S5B and S5C). Although this suggests broad functionality of *IL3RA* in the CNS, we focused on myeloid cells given their importance to MS plaque pathology and neuroinflammation and based on our findings in mice. Consistent with our murine data, *IL3RA* was expressed by myeloid cells in the WM and GM of control subjects and MS patients and in the plaques of MS patients (Figures 5E and S5D). Enumerating *IL3RA*-expressing cells (*IL3RA*$^+$) and measuring *IL3RA* showed that expression is significantly elevated in GM, WM, and plaque myeloid cells of MS patients relative to unaffected controls (Figure 5F). Importantly, *IL3RA* expression in all other CNS cell types remained unaltered in MS patients (Figure S5E). Further, we corroborated our data in a separate scRNA-seq dataset from a distinct cohort of human subjects[24] and found that among CSF leukocytes, myeloid cells express *IL3RA* most abundantly, and myeloid *IL3RA* expression was increased in MS patients (Figure S5G). These data suggest that the IL-3:IL-3RA axis is specifically and dynamically modulated in CNS myeloid cells during MS and may serve a critical function.

To further resolve myeloid cell functions in the relevant tissular microenvironment, we performed subclustering of myeloid cells in MS plaques and identified five clusters (Figure 5G). To assess the properties of each cluster, we conducted pathway analysis on enriched genes. This uncovered distinct functional characteristics for each cluster, including plaque myeloid clusters programmed for cytokine production (cluster 1), migration and chemotaxis (cluster 2), synapse pruning (cluster 3), phagocytosis (cluster 4), and synapse organization/brain development (cluster 5) (Figure S5H). We then quantified *IL3RA*$^+$ cells and *IL3RA* expression in each cluster and found that cluster 2—wired for myeloid cell migration, matrix remodeling, and chemotaxis (Figure 5H)—was solely and specifically enriched for *IL3RA* (Figure 5I). In agreement with our murine findings (Figure S4F), *MRC1* and *MERTK*, IL-3-controlled myeloid APC differentiation genes, were upregulated in cluster 2 while *C5AR1*, an IL-3-controlled undifferentiated monocytic marker, was downregulated (Figure 5H). This unbiased clustering revealed cluster 2 as enriched in *IL3RA*-expressing plaque myeloid cells programmed for immune cell recruitment and chemotaxis and is relevant to MS.

Next, to acquire a more targeted understanding of IL-3RA-controlled cell function and given our murine findings, we interrogated upregulated and downregulated genes and pathways in *IL3RA*-expressing myeloid cells residing in plaques. We found that *IL3RA*-expressing myeloid cells were enriched for chemotactic and migratory genes, including *CX3CR1*, *P2RY12*, *USP9Y*, *MAP4K1*, and *CCL3*, and programs associated with cell migration and chemotaxis (Figure 5J). Further, the most

Please cite this article in press as: Kiss et al., Interleukin-3 coordinates glial-peripheral immune crosstalk to incite multiple sclerosis, Immunity (2023), https://doi.org/10.1016/j.immunu.2023.04.013

CellPress

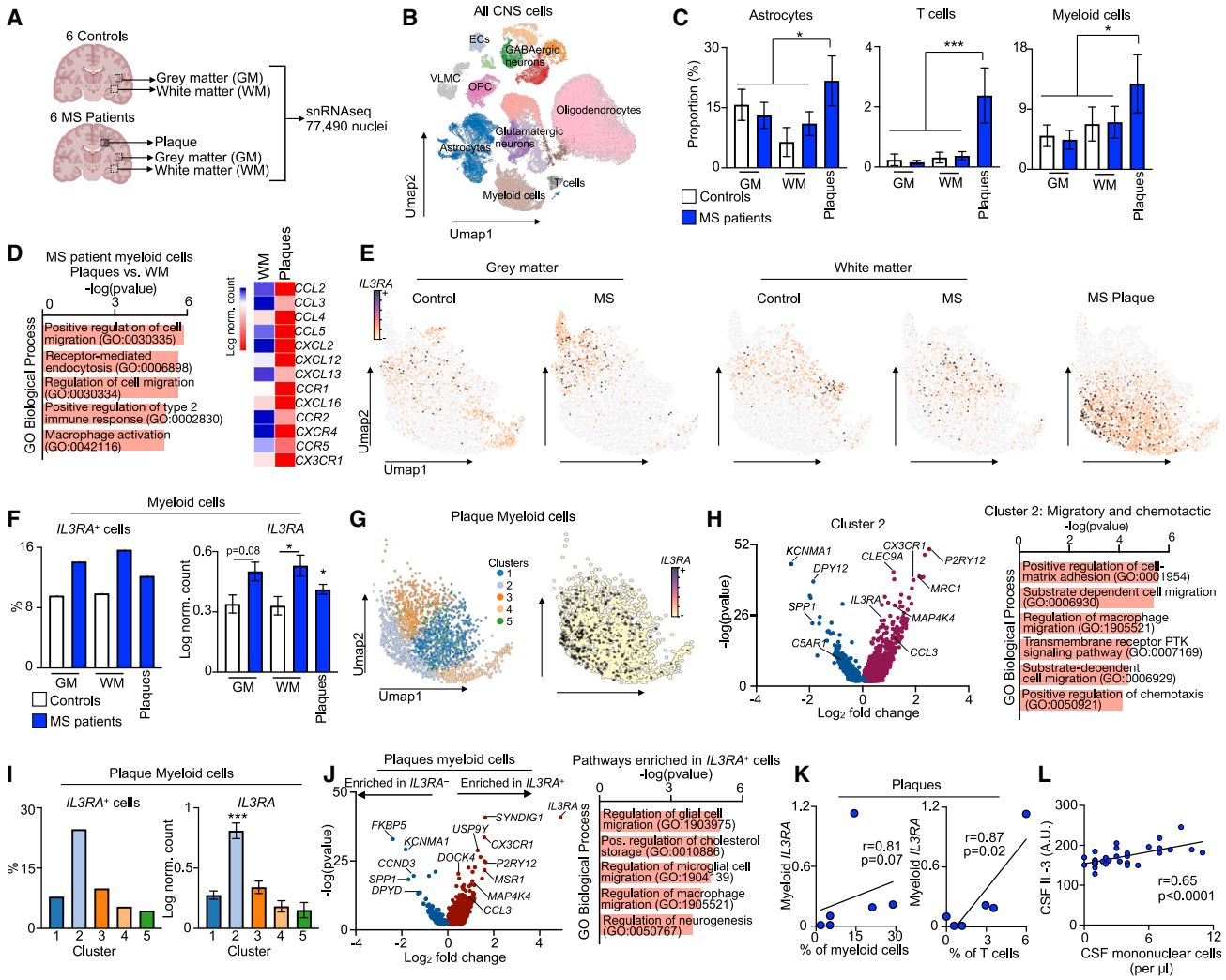

Figure 5. IL-3:IL-3RA promotes migratory and chemotactic myeloid cell subsets in CNS plaques of MS patients

(A) Schematic of human study and snRNA-seq analysis of white matter (WM) and gray matter (GM) from unaffected control subjects and MS patients along with plaques from MS patients.

(B) UMAP visualization of all CNS cells across all tissue regions and subjects.

(C) Proportion of astrocytes, T cells, and myeloid cells in white matter, gray matter, and plaque of control subjects and MS patients (one-way ANOVA).

(D) Pathway analysis of genes enriched in myeloid cells and expression of chemotactic genes and receptors in myeloid cells deriving from the plaques vs. adjacent white matter of MS patients.

(E) UMAP visualizations of *IL3RA*-expressing myeloid cells across tissue regions and subjects.

(F) Proportion of *IL3RA*-expressing myeloid cells (left) and relative myeloid *IL3RA* expression (right) across tissue regions and disease states (one-way ANOVA).

(G) UMAP visualization of myeloid clusters and *IL3RA* expression in MS plaques.

Q11 (H) Volcano plot of upregulated and downregulated genes in MS plaque myeloid cluster 2 and GO biological pathway analysis of upregulated genes.

(I) Proportion of *IL3RA*-expressing myeloid cells (left) and *IL3RA* expression (right) among myeloid clusters of MS plaques.

(J) Volcano plot of genes enriched in *IL3RA*-expressing and -non-expressing plaque myeloid cells, and pathway analysis of genes upregulated in *IL3RA*-expressing plaque myeloid cells.

(K) Correlation of plaque myeloid *IL3RA* expression with the proportion of plaque myeloid and T cells (Spearman correlation).

(L) Correlation of CSF IL-3 amount with CSF mononuclear cell abundance in MS patients (Spearman correlation).

n = 6 unaffected control and 6 MS patients, except in (L) n = 28 MS patients.

Mean ± SEM, *p < 0.05, **p < 0.01, and ***p < 0.001.

WM, white matter; GM, gray matter; MS, multiple sclerosis; CNS, central nervous system; UMAP, uniform manifold approximation and projection; ECs, endothelial cells; VLMCs, vascular leptomeningeal cells; OPC, oligodendrocyte progenitor cells; AU, arbitrary unit.

See also Figure S5.

Please cite this article in press as: Kiss et al., Interleukin-3 coordinates glial-peripheral immune crosstalk to incite multiple sclerosis, Immunity (2023), https://doi.org/10.1016/j.immuni.2023.04.013

highly downregulated genes in *IL3RA*$^{+}$ plaque myeloid cells, in comparison to *IL3RA*$^{-}$ cells, were *FKBP5*, a chaperone of the glucocorticoid receptor, and *KCNMA1*, an ion channel subunit critical to neurotransmitter release, and loss of function of these genes is strongly associated with demyelinating disease, neuromyelitis, and MS.[25,26] Together, these findings demonstrate that the CNS of MS patients, particularly in plaques, has more *IL3RA*-expressing myeloid cells and that IL-3RA plays an important role in the generation of antigen-presenting myeloid cells and their instigation of immune cell trafficking, chemotaxis, and migration programs.

To assess whether IL-3:IL-3RA associates with immune cell recruitment to the CNS in human MS, we correlated *IL3RA* expression by plaque myeloid cells with myeloid and T cell abundance in the plaques. We found a significant and positive correlation between plaque myeloid *IL3RA* expression and the number of plaque T cells and myeloid cells (Figure 5K). Finally, we returned to our human cohort in which we measured CSF IL-3 and found that IL-3 in the CSF of RRMS patients correlated positively and significantly with CSF mononuclear cell numbers (Figure 5L). In sum, these data support the hypothesis that IL-3:IL-3RA signaling mediates communication among ontologically distinct immune cell subsets in human MS plaques and, through the induction of chemotactic and recruitment programs, perpetuates neuroinflammation and disease severity (Figure S5I).

DISCUSSION

Inflammatory networks, glial cells, and infiltrating immune cells play consequential roles in neuroinflammation. However, little is known about the communication systems that coordinate cellular function and crosstalk in this diverse CNS ecosystem. Here, we have reported on IL-3-mediated central-peripheral immune communication in MS and CNS inflammation and position IL-3 as a pathogenic effector cytokine-growth factor. Our study identified both CNS-resident and infiltrating cells that generated IL-3 and responded to it. This integrated bidirectional network, we reveal, has a fundamental consequence on the programing and function of myeloid cell subsets in the CNS and in the clinical and pathological severity of MS.

Our data showed that resident astrocytes and infiltrated CD44^{hi}CD4^{+} effector T cells are the relevant sources of IL-3 in the inflamed CNS and that both microglia and peripherally derived myeloid cells (MHCII^{+} macrophages, MoDCs, and monocytes) respond to IL-3 by expressing IL-3Rα. IL-3 signaling instigated a chemotactic program by IL-3Rα^{+} myeloid cells that perpetuated immune cell recruitment to the CNS and worsened clinical severity. In humans, we found that IL-3 is present in the CSF and correlated with disease diagnosis and severity. Region-specific snRNA-seq of brain tissue from control subjects and MS patients revealed augmentation of *IL3RA* by myeloid cells in WM and GM and plaque tissue of MS patients and that *IL3RA*-expressing myeloid cells in the MS plaque represent a migratory and chemotactic subset that instigated immune cell recruitment to the CNS. Together, these findings identify IL-3:IL-3RA as a pathogenic axis that mediates bidirectional communication between peripherally derived immune cells and resident CNS glial cells, thereby exacerbating MS and neuroinflammation.

Our results begin to resolve IL-3 in CNS health and disease. Since its discovery decades ago, IL-3 has been associated with multiple inflammatory diseases; however, its role in the CNS and neuroinflammation has remained vastly understudied. Prior work from our group has established IL-3 involvement in AD.[11] In this context, IL-3 safeguards against AD by inciting microglial clustering and clearance of Aβ and tau. Here, we report that IL-3 is detrimental in MS and EAE, neuroinflammatory conditions defined by substantial recruitment of peripheral immune cells to the CNS where they contribute to disease pathology and severity. Our results show that IL-3-stimulated chemotactic and migratory programs aggravate neuroinflammation and MS severity. Yet, in AD, in which microglial migration toward and clearance of Aβ and tau resolve pathology, IL-3 ameliorates disease. These findings underscore the critical nuances of balanced inflammation and IL-3 in neurological disease: where instigation can be protective in one setting and harmful in another.

The fundamental actions of IL-3 in MS have, until now, been unclear. MS presents more often in females, and the *IL3RA* gene is encoded on the human X chromosome, perhaps indicating that homozygosity and/or increased expression of this gene contributes to disease development. Indeed, our data demonstrate that in comparatively healthy WM and GM tissue of MS patients, which are devoid of MS plaques, *IL3RA* expression is elevated relative to corresponding tissue from control subjects. Although prior research has suggested IL-3 may be involved in demyelinating disease,[12,13] these studies have been limited and reported directly contradictory findings. Here, we firmly establish a fundamental and pathogenic role for this cytokine in autoimmune neuroinflammation and MS, using generated and cell-specific murine models, multiregional snRNA-seq of the human CNS, and contemporary tools.

We position IL-3 as a paracrine modulator of myeloid cell recruitment and function through its local activities in the CNS. Myelopoiesis is heightened in MS and EAE[27]; however, we found that in MS, unlike in other inflammatory settings,[6] IL-3 does not serve as an endocrine amplifier of monocyte generation or hematopoiesis in distal compartments. Likewise, we did not find an impact of IL-3 on peripheral immune priming. The effects of IL-3 in MS and EAE appear to be local, and our data identified the effector organ, the CNS, as the consequential site for IL-3 production and action and reveal multifunctionality of the cytokine beyond leukocyte generation.

We present astrocytes and pro-inflammatory T cells as the two consequential sources of IL-3 in the CNS during EAE and employ cell-specific models to demonstrate their relevance. We characterize CD4^{+} T_H cell subsets that generate IL-3 in the inflamed CNS and show co-production of GM-CSF, IFN-γ, and IL-17A. IL-3 generation by CD4^{+} T cells might be directed by a pathogenic effector program or by inducible factors downstream of TCR and costimulatory signaling, but this requires formal evaluation in future studies.[28,29] Ultimately, our data reveal IL-3 as part of a pathogenic T cell signature. Further work will also be required to better characterize IL-3-producing astrocytes, including testing their transcriptional, metabolic, and biological programming and regional specificity in the CNS. Our observations that astrocytes generate IL-3 in the healthy CNS and that the cytokine is present in the CSF of healthy humans raise

Please cite this article in press as: Kiss et al., Interleukin-3 coordinates glial-peripheral immune crosstalk to incite multiple sclerosis, Immunity (2023), https://doi.org/10.1016/j.immuni.2023.04.013

questions about its role in brain homeostatic functioning. Additionally, our data identified multiple CNS cell types that express *IL3RA* in health and disease. Future studies will need to investigate IL-3 in brain health, development, and aging and to systematically resolve the role of IL-3RA in diverse CNS cells including neurons, oligodendrocytes, and ECs, among others.

MS currently has no cure, and patients are susceptible to developing severe disability and have shorter life expectancies. Targeting glial-peripheral signaling may be an effective therapeutic strategy,[17] and our data propose focusing on IL-3-mediated communication to curb immune cell infiltration, demyelination, and clinical symptoms. Biologics and small molecules targeting IL-3 signaling have been used in cancer therapy, and their application to MS treatment merits further exploration.[30–32] Whether targeting IL-3 or IL-3RA by pharmacological, biological, or genetic means, or identifying more appropriate downstream targets in the IL-3 axis, this pathway may offer an additional vista in drug development for MS and other neuroinflammatory conditions. Altogether, our data resolve IL-3 signaling in MS and identify the cytokine as a multifaceted actor that coordinates bidirectional communication among resident glia and infiltrating immune cells during CNS autoimmune inflammation.

Limitations of the study

Our study elevates IL-3 as a critical mediator of neuroinflammation in MS and its preclinical model. A limitation of our study is that we use a murine model of progressive MS that does not fully recapitulate the relapse and remitting features of clinical MS. Further investigations into the role of IL-3 and its therapeutic application in preclinical models of RRMS are warranted. Further, the stimuli and factors that induce astrocytic IL-3 production are unclear, and a granular investigation into the functional attributes of IL-3-producing astrocytes deserves to be explored. Our snRNA-seq analysis of human brain tissue was unable to identify IL-3-producing cells. This is common in astrocyte profiling and likely because the depth of our sequencing was not sufficient to detect this rare and quickly degraded transcript and that transcription of *Il3* occurs in discrete temporal windows dependent on stimuli and environment. Additional technologies that detect and profile rare astrocytic populations are becoming available (such as focused interrogation of cells by nucleic acid detection and sequencing, FIND-seq[33]) and can be used to interrogate IL-3-producing astrocytes. Finally, our data suggest that many cells in the CNS respond to IL-3. The contribution of *IL3RA*-expressing non-myeloid cells, such as neurons, oligodendrocytes, or ECs, to MS pathology was not explored here and should be tested.

STAR★METHODS

Detailed methods are provided in the online version of this paper and include the following:

- KEY RESOURCES TABLE
- RESOURCE AVAILABILITY
  - Lead contact
  - Materials availability
  - Data and code availability
- EXPERIMENTAL MODEL AND SUBJECT DETAILS
  - Mice
  - CRISPR-Cas9 generation of *Il3ra*$^{-/-}$ mice
  - Human CSF proteomic subjects
  - Human snRNAseq subjects
- METHOD DETAILS
  - In Vivo Interventions
  - Cells
  - Ex vivo cell cultures
  - Histopathology
  - Molecular Biology
  - Human CSF proteomics
  - Human snRNAseq
- QUANTIFICATION AND STATISTICAL ANALYSIS

SUPPLEMENTAL INFORMATION

Supplemental information can be found online at https://doi.org/10.1016/j.immuni.2023.04.013.

ACKNOWLEDGMENTS

We thank the HCI-CRM Flow Cytometry Core Facility at the Massachusetts General Hospital and the Flow Cytometry CoRE at the Icahn School of Medicine at Mount Sinai for assistance with cell sorting. We thank the Human Immune Monitoring Center at the Icahn School of Medicine at Mount Sinai for assistance in validation analysis. We thank K. Joyes for manuscript copy editing. This work was funded by the an Erwin Schrödinger Postdoctoral Fellowship J4645 by the Austrian Science Fund (to M.G.K.); National Institutes of Health (NIH) Ruth L. Kirschstein National Research Service Award Individual Predoctoral Fellowship F31HL147364 (to J.E.M.); NIH R35 HL139598, NIH R01 NS127808, and NIH R01 NS108419 (to M.N.); an MGH ECOR Howard M. Goodman Award (to B.P.K); NIH R01AG065582, R01AG067025, and R01AG050986 (to P.R.); NIH National Center for Advancing Translational Sciences UL1TR001873; Cure Alzheimer's Fund, NIH R35 HL135752, P01 HL131478, and the Patricia and Scott Eston MGH Research Scholar (to F.K.S.); NIH P01 HL142494 (to M.N., B.P.K., and F.K.S.); and NIH K99/R00 HL151750, R01 HL158534, and the Cure Alzheimer's Fund (to C.S.M.). Q13

AUTHOR CONTRIBUTIONS

Conceptualization, J.E.M., M.G.K., A.G.Y., A.A., M.N., F.P., P.R., F.K.S., and C.S.M.; data acquisition, M.G.K., J.E.M., A.G.Y., D.L., J.F.F., A.A., W.C.P., P.H., Y.I., V.R., C.T.C., H.J., W.J., A.N., J.D., J.D.H., S.G., and S.S.; data analysis, M.G.K., J.E.M., A.G.Y., D.L., A.A., V.R., and C.S.M.; methodology, K.A.C., B.P.K., D.L., J.K., and C.S.M.; generation of *Il3ra*$^{-/-}$ mice, K.A.C., B.P.K., and C.S.M.; supervision, S.K.-S., P.R., F.K.S., and C.S.M.; manuscript writing and perpetration, M.G.K., J.E.M., A.G.Y., and C.S.M.; manuscript editing, M.G.K., J.E.M., A.G.Y., D.L., J.F.F., A.A., W.C.P., K.A.C., Y.I., V.R., J.D., C.T.C., P.H., H.J., A.N., J.D.H., W.J., S.G., S.S., D.L., J.K., S.K.-S., M.N., B.P.K., F.P., P.R., F.K.S., and C.S.M.

DECLARATION OF INTERESTS

B.P.K. is an inventor on patents and/or patent applications filed by Mass General Brigham that describe genome engineering technologies. B.P.K. is a consultant for EcoR1 capital and is an advisor to Acrigen Biosciences, Life Edit Therapeutics, and Prime Medicine.

INCLUSION AND DIVERSITY Q8

We support inclusive, diverse, and equitable conduct of research.

Received: October 17, 2022
Revised: February 7, 2023
Accepted: April 12, 2023
Published: May 8, 2023

REFERENCES

1. Reich, D.S., Lucchinetti, C.F., and Calabresi, P.A. (2018). Multiple sclerosis. N. Engl. J. Med. *378*, 169–180. https://doi.org/10.1056/NEJMra1401483.
2. Baecher-Allan, C., Kaskow, B.J., and Weiner, H.L. (2018). Multiple sclerosis: mechanisms and immunotherapy. Neuron *97*, 742–768. https://doi.org/10.1016/j.neuron.2018.01.021.
3. Lassmann, H. (2018). Multiple sclerosis pathology. Cold Spring Harb. Perspect. Med. *8*. https://doi.org/10.1101/cshperspect.a028936.
4. McGinley, M.P., Goldschmidt, C.H., and Rae-Grant, A.D. (2021). Diagnosis and treatment of multiple sclerosis: a review. JAMA *325*, 765–779. https://doi.org/10.1001/jama.2020.26858.
5. Dougan, M., Dranoff, G., and Dougan, S.K. (2019). GM-CSF, IL-3, and IL-5 family of cytokines: regulators of inflammation. Immunity *50*, 796–811. https://doi.org/10.1016/j.immuni.2019.03.022.
6. Mindur, J.E., and Swirski, F.K. (2019). Growth factors as immunotherapeutic targets in cardiovascular disease. Arterioscler. Thromb. Vasc. Biol. *39*, 1275–1287. https://doi.org/10.1161/ATVBAHA.119.311994.
7. Weber, G.F., Chousterman, B.G., He, S., Fenn, A.M., Nairz, M., Anzai, A., Brenner, T., Uhle, F., Iwamoto, Y., Robbins, C.S., et al. (2015). Interleukin-3 amplifies acute inflammation and is a potential therapeutic target in sepsis. Science *347*, 1260–1265. https://doi.org/10.1126/science.aaa4268.
8. Robbins, C.S., Chudnovskiy, A., Rauch, P.J., Figueiredo, J.L., Iwamoto, Y., Gorbatov, R., Etzrodt, M., Weber, G.F., Ueno, T., Van Rooijen, N., et al. (2012). Extramedullary hematopoiesis generates Ly-6C high monocytes that infiltrate atherosclerotic lesions. Circulation *125*, 364–374. https://doi.org/10.1161/CIRCULATIONAHA.111.061986.
9. Renner, K., Hermann, F.J., Schmidbauer, K., Talke, Y., Rodriguez Gomez, M., Schiechl, G., Schlossmann, J., Brühl, H., Anders, H.J., and Mack, M. (2015). IL-3 contributes to development of lupus nephritis in MRL/lpr mice. Kidney Int. *88*, 1088–1098. https://doi.org/10.1038/ki.2015.196.
10. Srivastava, R.K., Tomar, G.B., Barhanpurkar, A.P., Gupta, N., Pote, S.T., Mishra, G.C., and Wani, M.R. (2011). IL-3 attenuates collagen-induced arthritis by modulating the development of Foxp3+ regulatory T cells. J. Immunol. *186*, 2262–2272. https://doi.org/10.4049/jimmunol.1002691.
11. McAlpine, C.S., Park, J., Griciuc, A., Kim, E., Choi, S.H., Iwamoto, Y., Kiss, M.G., Christie, K.A., Vinegoni, C., Poller, W.C., et al. (2021). Astrocytic interleukin-3 programs microglia and limits Alzheimer's disease. Nature *595*, 701–706. https://doi.org/10.1038/s41586-021-03734-6.
12. Renner, K., Hellerbrand, S., Hermann, F., Riedhammer, C., Talke, Y., Schiechl, G., Rodriguez Gomez, M.R., Kutzi, S., Halbritter, D., Goebel, N., et al. (2016). IL-3 promotes the development of experimental autoimmune encephalitis. JCI Insight *1*. e87157. https://doi.org/10.1172/jci.insight.87157.
13. Lee, P.W., Xin, M.K., Pei, W., Yang, Y., and Lovett-Racke, A.E. (2018). IL-3 is a marker of encephalitogenic T cells, but not essential for CNS autoimmunity. Front. Immunol. *9*, 1255. https://doi.org/10.3389/fimmu.2018.01255.
14. Chiang, C.S., Powell, H.C., Gold, L.H., Samimi, A., and Campbell, I.L. (1996). Macrophage/microglial-mediated primary demyelination and motor disease induced by the central nervous system production of interleukin-3 in transgenic mice. J. Clin. Invest. *97*, 1512–1524. https://doi.org/10.1172/JCI118574.
15. Powell, H.C., Garrett, R.S., Brett, F.M., Chiang, C.S., Chen, E., Masliah, E., and Campbell, I.L. (1999). Response of glia, mast cells and the blood brain barrier, in transgenic mice expressing interleukin-3 in astrocytes, an experimental model for CNS demyelination. Brain Pathol. *9*, 219–235. https://doi.org/10.1111/j.1750-3639.1999.tb00220.x.
16. Chavany, C., Vicario-Abejón, C., Miller, G., and Jendoubi, M. (1998). Transgenic mice for interleukin 3 develop motor neuron degeneration associated with autoimmune reaction against spinal cord motor neurons. Proc. Natl. Acad. Sci. USA *95*, 11354–11359. https://doi.org/10.1073/pnas.95.19.11354.
17. Linnerbauer, M., Wheeler, M.A., and Quintana, F.J. (2020). Astrocyte crosstalk in CNS inflammation. Neuron *108*, 608–622. https://doi.org/10.1016/j.neuron.2020.08.012.
18. Mosleth, E.F., Vedeler, C.A., Liland, K.H., McLeod, A., Bringeland, G.H., Kroondijk, L., Berven, F.S., Lysenko, A., Rawlings, C.J., Eid, K.E.-H., et al. (2021). Cerebrospinal fluid proteome shows disrupted neuronal development in multiple sclerosis. Sci. Rep. *11*, 4087. https://doi.org/10.1038/s41598-021-82388-w.
19. Stangel, M., Fredrikson, S., Meinl, E., Petzold, A., Stüve, O., and Tumani, H. (2013). The utility of cerebrospinal fluid analysis in patients with multiple sclerosis. Nat. Rev. Neurol. *9*, 267–276. https://doi.org/10.1038/nrneurol.2013.41.
20. Mendel, I., Kerlero de Rosbo, N., and Ben-Nun, A. (1995). A myelin oligodendrocyte glycoprotein peptide induces typical chronic experimental autoimmune encephalomyelitis in H-2b mice: fine specificity and T cell receptor V beta expression of encephalitogenic T cells. Eur. J. Immunol. *25*, 1951–1959. https://doi.org/10.1002/eji.1830250723.
21. Constantinescu, C.S., Farooqi, N., O'Brien, K., and Gran, B. (2011). Experimental autoimmune encephalomyelitis (EAE) as a model for multiple sclerosis (MS). Br. J. Pharmacol. *164*, 1079–1106. https://doi.org/10.1111/j.1476-5381.2011.01302.x.
22. Caravagna, C., Jaouën, A., Desplat-Jégo, S., Fenrich, K.K., Bergot, E., Luche, H., Grenot, P., Rougon, G., Malissen, M., and Debarbieux, F. (2018). Diversity of innate immune cell subsets across spatial and temporal scales in an EAE mouse model. Sci. Rep. *8*, 5146. https://doi.org/10.1038/s41598-018-22872-y.
23. Greiner, T., and Kipp, M. (2021). What guides peripheral immune cells into the central nervous system? Cells *10*. https://doi.org/10.3390/cells10082041.
24. Schafflick, D., Xu, C.A., Hartlehnert, M., Cole, M., Schulte-Mecklenbeck, A., Lautwein, T., Wolbert, J., Heming, M., Meuth, S.G., Kuhlmann, T., et al. (2020). Integrated single cell analysis of blood and cerebrospinal fluid leukocytes in multiple sclerosis. Nat. Commun. *11*, 247. https://doi.org/10.1038/s41467-019-14118-w.
25. Bechmann, L., Busse, K., Stoppe, M., Cotte, S., Ettrich, B., and Then Bergh, F. (2014). Corticosteroid receptor expression and in vivo glucocorticoid sensitivity in multiple sclerosis. J. Neuroimmunol. *276*, 159–165. https://doi.org/10.1016/j.jneuroim.2014.07.004.
26. Umeton, R., Bellucci, G., Bigi, R., Romano, S., Buscarinu, M.C., Reniè, R., Rinaldi, V., Pizzolato Umeton, R., Morena, E., Romano, C., et al. (2022). Multiple sclerosis genetic and non-genetic factors interact through the transient transcriptome. Sci. Rep. *12*, 7536. https://doi.org/10.1038/s41598-022-11444-w.
27. Shi, K., Li, H., Chang, T., He, W., Kong, Y., Qi, C., Li, R., Huang, H., Zhu, Z., Zheng, P., et al. (2022). Bone marrow hematopoiesis drives multiple sclerosis progression. Cell *185*. 2234.e17–2247.e17. https://doi.org/10.1016/j.cell.2022.05.020.
28. Krishnarajah, S., and Becher, B. (2022). T(H) cells and cytokines in encephalitogenic disorders. Front. Immunol. *13*. 822919. https://doi.org/10.3389/fimmu.2022.822919.
29. Wagner, C.A., Roqué, P.J., and Goverman, J.M. (2020). Pathogenic T cell cytokines in multiple sclerosis. J. Exp. Med. *217*. https://doi.org/10.1084/jem.20190460.
30. Palmeri, S., Leonardi, V., Danova, M., Porta, C., Ferrari, S., Fincato, G., and Citarrella, P. (1999). Prospective, randomized trial of sequential interleukin-3 and granulocyte- or granulocyte-macrophage colony-stimulating factor after standard-dose chemotherapy in cancer patients. Haematologica *84*, 1016–1023.
31. Ballestrero, A., Ferrando, F., Garuti, A., Basta, P., Gonella, R., Stura, P., Mela, G.S., Sessarego, M., Gobbi, M., and Patrone, F. (1999). Comparative effects of three cytokine regimens after high-dose cyclophosphamide: granulocyte colony-stimulating factor, granulocyte-macrophage colony-stimulating factor (GM-CSF), and sequential interleukin-3 and GM-CSF. J. Clin. Oncol. *17*, 1296. https://doi.org/10.1200/JCO.1999.17.4.1296.

32. He, S.Z., Busfield, S., Ritchie, D.S., Hertzberg, M.S., Durrant, S., Lewis, I.D., Marlton, P., McLachlan, A.J., Kerridge, I., Bradstock, K.F., et al. (2015). A phase 1 study of the safety, pharmacokinetics and anti-leukemic activity of the anti-CD123 monoclonal antibody CSL360 in relapsed, refractory or high-risk acute myeloid leukemia. Leuk. Lymphoma *56*, 1406–1415. https://doi.org/10.3109/10428194.2014.956316.

33. Clark, I.C., Wheeler, M.A., Lee, H.G., Li, Z., Sanmarco, L.M., Thaploo, S., Polonio, C.M., Shin, S.W., Scalisi, G., Henry, A.R., et al. (2023). Identification of astrocyte regulators by nucleic acid cytometry. Nature *614*, 326–333. https://doi.org/10.1038/s41586-022-05613-0.

34. Anzai, A., Mindur, J.E., Halle, L., Sano, S., Choi, J.L., He, S., McAlpine, C.S., Chan, C.T., Kahles, F., Valet, C., et al. (2019). Self-reactive CD4+ IL-3+ T cells amplify autoimmune inflammation in myocarditis by inciting monocyte chemotaxis. J. Exp. Med. *216*, 369–383. https://doi.org/10.1084/jem.20180722.

35. Doench, J.G., Fusi, N., Sullender, M., Hegde, M., Vaimberg, E.W., Donovan, K.F., Smith, I., Tothova, Z., Wilen, C., Orchard, R., et al. (2016). Optimized sgRNA design to maximize activity and minimize off-target effects of CRISPR-Cas9. Nat. Biotechnol. *34*, 184–191. https://doi.org/10.1038/nbt.3437.

36. Bae, S., Park, J., and Kim, J.S. (2014). Cas-OFFinder: a fast and versatile algorithm that searches for potential off-target sites of Cas9 RNA-guided endonucleases. Bioinformatics *30*, 1473–1475. https://doi.org/10.1093/bioinformatics/btu048.

37. Conant, D., Hsiau, T., Rossi, N., Oki, J., Maures, T., Waite, K., Yang, J., Joshi, S., Kelso, R., Holden, K., et al. (2022). Inference of CRISPR edits from sanger trace data. CRISPR J. *5*, 123–130. https://doi.org/10.1089/crispr.2021.0113.

38. Kleinstiver, B.P., Sousa, A.A., Walton, R.T., Tak, Y.E., Hsu, J.Y., Clement, K., Welch, M.M., Horng, J.E., Malagon-Lopez, J., Scarfò, I., et al. (2019). Engineered CRISPR–Cas12a variants with increased activities and improved targeting ranges for gene, epigenetic and base editing. Nat. Biotechnol. *37*, 276–282. https://doi.org/10.1038/s41587-018-0011-0.

39. Rohland, N., and Reich, D. (2012). Cost-effective, high-throughput DNA sequencing libraries for multiplexed target capture. Genome Res. *22*, 939–946. https://doi.org/10.1101/gr.128124.111.

40. Blond, D., Campbell, S.J., Butchart, A.G., Perry, V.H., and Anthony, D.C. (2002). Differential induction of interleukin-1beta and tumour necrosis factor-alpha may account for specific patterns of leukocyte recruitment in the brain. Brain Res. *958*, 89–99. https://doi.org/10.1016/s0006-8993(02)03473-x.

41. McCluskey, L., Campbell, S., Anthony, D., and Allan, S.M. (2008). Inflammatory responses in the rat brain in response to different methods of intra-cerebral administration. J. Neuroimmunol. *194*, 27–33. https://doi.org/10.1016/j.jneuroim.2007.11.009.

42. Dickens, A.M., Tovar-Y-Romo, L.B., Yoo, S.W., Trout, A.L., Bae, M., Kanmogne, M., Megra, B., Williams, D.W., Witwer, K.W., Gacias, M., et al. (2017). Astrocyte-shed extracellular vesicles regulate the peripheral leukocyte response to inflammatory brain lesions. Sci. Signal. *10*. https://doi.org/10.1126/scisignal.aai7696.

43. Probert, F., Yeo, T., Zhou, Y., Sealey, M., Arora, S., Palace, J., Claridge, T.D.W., Hillenbrand, R., Oechtering, J., Leppert, D., et al. (2021). Integrative biochemical, proteomics and metabolomics cerebrospinal fluid biomarkers predict clinical conversion to multiple sclerosis. Brain Commun. *3*. fcab084. https://doi.org/10.1093/braincomms/fcab084.

44. Li, B., Gould, J., Yang, Y., Sarkizova, S., Tabaka, M., Ashenberg, O., Rosen, Y., Slyper, M., Kowalczyk, M.S., Villani, A.C., et al. (2020). Cumulus provides cloud-based data analysis for large-scale single-cell and single-nucleus RNA-seq. Nat. Methods *17*, 793–798. https://doi.org/10.1038/s41592-020-0905-x.

45. Wolf, F.A., Angerer, P., and Theis, F.J. (2018). SCANPY: large-scale single-cell gene expression data analysis. Genome Biol. *19*, 15. https://doi.org/10.1186/s13059-017-1382-0.

46. Korsunsky, I., Millard, N., Fan, J., Slowikowski, K., Zhang, F., Wei, K., Baglaenko, Y., Brenner, M., Loh, P.R., and Raychaudhuri, S. (2019). Fast, sensitive and accurate integration of single-cell data with Harmony. Nat. Methods *16*, 1289–1296. https://doi.org/10.1038/s41592-019-0619-0.

Please cite this article in press as: Kiss et al., Interleukin-3 coordinates glial-peripheral immune crosstalk to incite multiple sclerosis, Immunity (2023), https://doi.org/10.1016/j.immuni.2023.04.013

STAR★METHODS

KEY RESOURCES TABLE

REAGENT or RESOURCE	SOURCE	IDENTIFIER
Antibodies		
anti-CD45 BUV737 (clone 30-F11)	BD Biosciences	Cat# 748371
anti-CD45 BV711 (clone 30-F11)	BioLegend	Cat# 103147
anti-CD3 (clone 17A2) FITC	BioLegend	Cat# 100204
anti-CD3ε (clone 145-2C11) PE	BioLegend	Cat# 100308
anti-CD4 (clone RM4-5) FITC	BioLegend	Cat# 100510
anti-CD4 (clone RM4-5) PE-Cyanine7	BioLegend	Cat# 100528
anti-CD8a (clone 53–6.7) Alexa Fluor 700	BioLegend	Cat# 100730
anti-CD90.2 (clone 53-2.1) PE	BioLegend	Cat# 140308
anti-CD19 (clone 6D5)	BioLegend	Cat# 115538
anti-B220 (clone RA3-6B2) BV785	BioLegend	Cat# 103246
anti-Ly6G (clone 1A8) BV421	BioLegend	Cat# 127645
anti-Ly-6C (AL-21) BV605	BD Biosciences	Cat# 563011
anti-I-A/I-E (MHCII; clone M5/114.15.2) Alexa Fluor 700	BioLegend	Cat# 107622
anti-CD11b (clone M1/70) APC/Cyanine7	BioLegend	Cat# 101226
anti-CD11c (cloneClone HL3) PerCP-Cy5.5	BD Biosciences	Cat# 560584
anti-CD44 (clone IM7) PE-Cyanine7	BioLegend	Cat# 103030
anti-CD62L (clone MEL-14) Alexa Fluor 700	BioLegend	Cat# 104426
anti-CD64 (clone X54-5/7.1) PE	BioLegend	Cat# 139304
anti-CD80 (clone 16-10A1) FITC	BioLegend	Cat# 104706
anti-CD86 (clone GL-1) PE/Cyanine7	BioLegend	Cat# 105014
anti-OX40L (clone RM134L) APC	BioLegend	Cat# 108812
anti-CD69 (clone H1.2F3) BV711	BioLegend	Cat# 104537
anti-CD49d (integrin α4; clone R1-2) PE	BioLegend	Cat# 103608
Anti-Ly6G (clone 1AB-Ly6g) PerCP/ eFluor710	Thermo Fisher Sci.	Cat# 46-9668-82
Anti-I-A/I-E (MHCII; clone M5/114.15.2) BUV495	BD Biosciences	Cat# 750281
anti-Ki67 (clone SolA15) PE	ThermoFisher Sci.	12-5698-82
anti-IL-3Rα (CD123; clone REA114)	Miltenyi Biotec	Cat# 130-102-583
anti-F4/80 (clone BM8) APC/Cyanine7	BioLegend	Cat# 123118
anti-CD115 (CSF-1R; clone AFS98) BV605	BioLegend	Cat# 135517
anti-CX3CR1 (clone SA011F11) PE-Cyanine7	BioLegend	Cat# 149016
anti-IL-3 (clone MP2-8F8)	BD Biosciences	Cat# 554383
anti-IFNγ (clone XMG1.2) BV605	BioLegend	Cat# 505840
anti-IL-17A (clone TC11-18H10.1) APC/ Cyanine7	BioLegend	Cat# 506922
anti-GM-CSF (clone MP1-22E9) BV421	BD Biosciences	Cat# 564747
anti-CD11b (clone M1/70) BUV805	BD Biosciences	Cat# 741934
anti-ACSA2 (clone REA969) APC	Miltenyi Biotec	Cat# 130-116-245
anti-CD19 (clone 1D3) BUV661	BD Biosciences	Cat# 612971
anti-CD8 (clone 53-6.7) PE-Dazzle594	BioLegend	Cat# 100762
anti-IL3	BioLegend	Cat# 503902
AF488 anti-GFAP	eBioscience	Cat# 53-9892

(*Continued on next page*)

Please cite this article in press as: Kiss et al., Interleukin-3 coordinates glial-peripheral immune crosstalk to incite multiple sclerosis, Immunity (2023), https://doi.org/10.1016/j.immuni.2023.04.013

Continued

REAGENT or RESOURCE	SOURCE	IDENTIFIER
Anti-IL3Rα	US Biological	Cat# 141039
anti-CD11b	BD Biosciences	Cat# 550282
anti-rabbit IgG	Vector Laboratories	Cat# BA-1000
anti-rat IgG	Thermo Fisher Scientific	Cat# A-11006
anti-rat IgG	Vector Laboratories	Cat# BA-4001
Mouse anti-IL4	BioLegend	Cat# 504122
Mouse anti-CD28	Thermo Fisher Sci.	Cat# 16-0281-82
Mouse anti-CD3ε	Thermo Fisher Sci.	Cat# 16-0031-82
Mouse anti-IL12	Thermo Fisher Sci.	Cat# 45-7123-80
Mouse anti- IFNy	BioLegend	Cat# 513208
Biological samples		
Human brain tissue	Human Brain and Spinal Fluid Resource Center, UCLA	N/A
Human CSF samples	Department of Neurology of the University Hospital Basel	N/A
Chemicals, peptides, and recombinant proteins		
DAPI	Thermoscientific	Cat# 62248
IL-3	Peprotech	Cat# 213-13
IL-12	Peprotech	Cat#210-12
TGF-β1	Peprotech	Cat# 100-21
IL-6	Peprotech	Cat# 216-16
IL-23	Peprotech	Cat# 200-23
IL-2	Peprotech	Cat# 21212
IL-1β	BioLegend	Cat# 575102
Tamoxifen	Sigma Aldrich	T5648
Critical commercial assays		
RNeasy Mini kit	Qiagen	Cat# 74104
RNeasy Micro Kit	Qiagen	Cat# 74004
High-Capacity cDNA Reverse Transcription Kit	Thermo Fisher	Cat# 4368814
MOG35-55/CFA Emulsion PTX Hooke KitTM	Hooke Laboratories	Cat# EK-2110
Luxol Fast Blue Stain Kit	Abcam	Cat# ab150675
IL-3 ELISA kit	Boster Biological	Cat# EK0403
IFNγ ELISA kit	R&D Systems	Cat# MIF00
IL17A ELISA kit	R&D Systems	Cat# M1700
GM-CSF ELISA kit	R&D Systems	Cat# MGM00
CCL2 ELISA Kit	R&D Systems	Cat# MJE00B
Zombie Aqua Fixable Viability Kit	BioLegend	423102
eBioscience FoxP3/ Transcription Factor Staining Buffer Set	Thermo Fisher Sci.	00-5523-00
Fixation/Permeabilization Kit with BD GolgiPlug	BD Biosciences	555028
CountBright Absolute Counting Beads	Thermo Fisher Sci.	C36950
Monocyte Isolation Kit	Miltenyi Biotec	130-100-629
Chromium Single Cell 3' Reagent Kits v3	10x Genomics	Cat# 1000075
Chromium i7 Sample Index Plate	10x Genomics	Cat# 220103
Kapa Library Quantification Kit	KAPA Biosystems	Cat# KK4873
Tapestation D5000 ScreenTape	Agilent Technologies	Cat# 5067-5588

(*Continued on next page*)

Please cite this article in press as: Kiss et al., Interleukin-3 coordinates glial-peripheral immune crosstalk to incite multiple sclerosis, Immunity (2023), https://doi.org/10.1016/j.immuni.2023.04.013

Continued

REAGENT or RESOURCE	SOURCE	IDENTIFIER
Tapestation D5000 Reagents	Agilent Technologies	Cat# 5067-5589
Deposited data		
Single nuclear RNA-seq	Gene Expression omnibus	GSE227781
Experimental models: Organisms/strains		
C57BL/6J	The Jackson Laboratories	Strain# 000664
Aldh1l1cre^{Ert2}	The Jackson Laboratories	Strain# 031008
Cd4cre	The Jackson Laboratories	Strain# 022071
Il3$^{-/-}$	The Jackson Laboratories	Strain# 026277
IL3$^{GFPfl/fl}$	McAlpine lab	N/A
Il3rα$^{-/-}$	McAlpine lab	N/A
Oligonucleotides		
Il3 (Mm00439631_m1)	Thermo Fisher	Cat# 4331182
Ccl2 (Mm00441242_m1)	Thermo Fisher	Cat# 4331182
Ccl5 (Mm01302427_m1)	Thermo Fisher	Cat# 4331182
Ccl7 (Mm00443113_m1)	Thermo Fisher	Cat# 4331182
Ccl12 (Mm01617100_m1)	Thermo Fisher	Cat# 4331182
Il3rα (Mm00434273_m1)	Thermo Fisher	Cat# 4331182
Csf2rb (Mm00655745_m1)	Thermo Fisher	Cat# 4331182
Ccr7 (Mm99999130_s1)	Thermo Fisher	Cat# 4331182
Flt3 (Mm00439016_m1)	Thermo Fisher	Cat# 4331182
Kit (Mm00445212_m1)	Thermo Fisher	Cat# 4331182
Spp1 (Mm00436767_m1)	Thermo Fisher	Cat# 4331182
C5ar1 (Mm00500292_s1)	Thermo Fisher	Cat# 4331182
Irf4 (Mm00516431_m1)	Thermo Fisher	Cat# 4331182
Ly6c2 (Mm00841873_m1)	Thermo Fisher	Cat# 4331182
Cd209a (Mm00460067_m1)	Thermo Fisher	Cat# 4331182
Fcgr1 (Mm00438874_m1)	Thermo Fisher	Cat# 4331182
Zbtb46 (Mm00511327_m1)	Thermo Fisher	Cat# 4331182
Actb (Mm00607939_s1)	Thermo Fisher	Cat# 4331182
Software and algorithms		
NDP.view 2	Hamamatsu Photonics	www.hamamatsu.com
FlowJo v10	FlowJo	www.flowjo.com
GraphPad Prism v9	GraphPad Software	www.graphpad.com
BioRender	BioRender	www.biorender.com
SomaScan	SomaLogic Inc	www.somalogic.com
Cell Ranger	10x Genomics	v7.0.0
Pegasus	https://github.com/lilab-bcb/pegasus	v1.7.0
Scanpy	https://github.com/scverse/scanpy	v1.8.2
Anndata	https://github.com/scverse/anndata	v0.8.0
Numpy	https://github.com/numpy/numpy	v1.21.5
Scipy	https://github.com/scipy/scipy	v1.8.0
Pandas	https://github.com/pandas-dev/pandas	v1.4.1
Umap	https://github.com/lmcinnes/umap	v0.5.2
scikit-learn	https://github.com/scikit-learn/scikit-learn	v1.0.2
Statsmodels	https://github.com/statsmodels/statsmodels	v0.13.2
python-igraph	https://github.com/igraph/python-igraph	v0.9.9

Please cite this article in press as: Kiss et al., Interleukin-3 coordinates glial-peripheral immune crosstalk to incite multiple sclerosis, Immunity (2023), https://doi.org/10.1016/j.immuni.2023.04.013

RESOURCE AVAILABILITY

Lead contact

Further information and requests for resources and reagents should be directed to and will be fulfilled by the lead contact, Cameron S. McAlpine (Cameron.mcalpine@mssm.edu).

Materials availability

Mouse lines generated in this study are available from the lead contact upon request. Distribution of mouse lines may require a material transfer agreement (MTA).

Data and code availability

- Single nuclear RNA-seq data have been deposited at GEO under the accession GSE227781 and are publicly available as of the date of publication. Accession numbers are listed in the key resources table.
- Any additional information required to reanalyze the data reported in this paper is available from the lead contact upon request.

EXPERIMENTAL MODEL AND SUBJECT DETAILS

Mice

Wild-type C57BL/6J, *Aldh1l1cre*^{Ert2}, and *Cd4cre* mice were purchased from the Jackson Laboratory. C57BL/6J mice were also bred in-house. *Il3*$^{-/-}$ mice were bred in house.[7,34] *IL3*$^{GFPfl/fl}$ mice were bred in house and their generation has been previously described.[11] Age- and sex- matched mice were used. Where appropriate, mice were randomly assigned to interventions. Littermate controls were used in all cell-specific genetic deletion studies. Experiments were initiated when mice were 10-12 weeks old. All mice had free access to food and water. For EAE experiments, mice were single housed. All animal protocols were approved by the Animal Review Committee at the Massachusetts General Hospital (protocol nos. 2011N000035 and 2015N000044) and/or the Icahn School of Medicine at Mount Sinai (protocol nos. PROTO202100023 and PROTO202000262) and were in compliance with relevant ethical regulations.

CRISPR-Cas9 generation of *Il3ra*$^{-/-}$ mice

To generate *Il3ra*$^{-/-}$ mice on the C57BL/6J background, two SpCas9 guide RNAs (gRNAs) were designed to target genomic regions within the first intron and 3' of the stop codon of the mouse *Il3ra* gene using on-target and off-target prediction software.[35,36] The on-target activities of candidate gRNAs were tested by microinjection of ribonucleoprotein (RNP) complexes comprised of TrueCut Cas9 v2 (ThermoFisher) and synthetic gRNAs (Synthego) into mouse zygotes. All microinjections were performed at the Genome Modification Facility (Harvard University). Injected zygotes developed to the blastocyst stage prior to undergoing genomic DNA extraction. To confirm the genome editing efficiencies of candidate gRNAs at the mouse *Il3ra* locus, the target genomic regions were amplified by PCR using the following forward and reverse amplicon primers: oBK8664 (forward; 5'-GATGATGTCATTCTCACCCCCAGATGTC-3') and oBK8667 (reverse; 5'-TGCAGGTTCTGGATGGGCGTGGTC-3') to sequence intron 1 targets for *Il3ra*; and oBK8668 (forward; 5'-GGACAGGAAGTGACACTGGGGGTCAG-3') and oBK8671 (reverse; 5'-GCAATCCCTCTGTCTCAGCTCCTG-3') to sequence stop codon targets for *Il3ra*. Amplicons were sent for Sanger sequencing and the approximate level of on-target activity was determined using ICE.[37] The most effective gRNAs of each pair examined (mIl3ra-1: spacer sequence: GGGACCAATGATGTCACCTA, and PAM: GGG; and mIL3ra-STOP-2: spacer sequence: AGACGCCTGAGAACTGTGTG, and PAM: GGG, which target the first intron and 3' of the stop codon of the *Il3ra* gene, respectively) were then used for microinjections to generate *Il3ra*$^{-/-}$ mice by excision of a 7712 bp region of genomic DNA spanning *Il3ra* introns 2-11 (Figure S4C). Injected embryos were implanted into pseudopregnant recipients, and *Il3ra* gene-targeted mice were genotyped at 3 weeks of age. To genotype mice, genomic DNA was extracted from tail snips in 200 μL of tail lysis buffer (100 mM Tris-HCl, 200mM NaCl, 5mM EDTA, 0.05% SDS, 12.5 mM DTT, 1.4 μg/μl Proteinase K (New England Biolabs) via ~16-hour incubation at 55 ºC. Lysates were cleaned up using 0.7x paramagnetic beads prepared as previously described.[38,39] Subsequent *Il3ra*$^{-/-}$ mice were genotyped by PCR using the following forward and reverse amplicon primers: oBK8665 (forward; 5'- CCCTAAGCTCTTCCCTTCTTGTTGGC-3') and oBK8670 (reverse; 5'-CCTTCAGAGCCCCACTTCCTGTC GAAG-3') to detect the *Il3ra* ablated allele; and oBK8668 (forward; 5'- GGACAGGAAGTGACACTGGGGGTCAG-3') and oKAC236 (reverse; 5'- CCAGAAGGAACCCGAGCTTCATC-3') to detect the wild-type allele. Deletion of the targeted *Il3ra* genomic locus was confirmed by Sanger sequencing using the following primers: oKAC233 (forward; 5'-GGACCATGACAGGAACCAGAAGC-3') and oKAC237 (reverse; 5'-GTTACAACACCTAGAAGTAGTACCTCCTC-3'). One founder mouse with successful deletion of *Il3ra* exons 2-11 was selected for further breeding in-house with C57BL/6J mice.

Human CSF proteomic subjects

CSF samples were collected from study participants in the Department of Neurology of the University Hospital Basel. Participants were characterized as (i) healthy controls with no evidence of neurological disease (20 females and 15 males, age: 43.5±2.1 years), (ii) patients with clinical defined RRMS (29 females and 7 males, age: 36.4±1.6 years), or (iii) patients that have experienced a single clinical episode suggestive of MS, known as clinically isolated syndrome (CIS). CIS patients were further differentiated into those who

Please cite this article in press as: Kiss et al., Interleukin-3 coordinates glial-peripheral immune crosstalk to incite multiple sclerosis, Immunity (2023), https://doi.org/10.1016/j.immuni.2023.04.013

developed clinically defined MS (converters, 17 females and 5 males, age: 36.4±2.0), according to the Poser criteria, during follow-up of at least 2 years, and those that remained stable (non-converters, 21 females and 11 males, age: 31.3±2.1). Patients with neuromyelitis optica, a history of progressive disease, active systemic infection, or undergoing steroid treatment at the time of sampling, were excluded from the study. Written informed consent was obtained from all participants according to the Declaration of Helskinki. Ethical approval was obtained by local ethics and IRB committee for use of deidentified samples. For RRMS patients, some samples were collected during remission (58% of RRMS samples) and others during a relapse (42% of RRMS samples).

Human snRNAseq subjects

Twelve fresh frozen brain tissue specimens, consisting of 6 MS cases (4 males and 2 females, age: 64±6) and 6 unaffected controls (4 males and 2 females, age: 63±3.3), were obtained through the NIH NeuroBiobank from the Human Brain and Spinal Fluid Resource Center, UCLA. All neuropsychological, diagnostic, and autopsy protocols were approved by the respective Institutional Review Boards. For the cases, each specimen contained a visible plaque and adjacent normal-appearing white matter (NAWM) and normal-appearing gray matter (NAGM). The unaffected control specimens consisted of NAWM and NAGM.

METHOD DETAILS

In Vivo Interventions

EAE induction and scoring

EAE was induced using the MOG35-55/CFA Emulsion PTX Hooke Kit™ (Cat. No. EK-2110; Hooke Laboratories, Inc.). Briefly, mice were subcutaneously injected in the flank with 100 μg myelin oligodendrocyte glycoprotein peptide residues 35-55 (MOG35-55: MEVGWYRSPFSRVVHLYRNGK) emulsified in complete Freund's adjuvant (CFA) containing 2-5 mg/mL of heat-killed *Mycobacterium tuberculosis H37Ra* on day 0. Mice also received between 80-100 ng pertussis toxin (PTX) in PBS via intraperitoneal injection on days 0 and 2. Mice were monitored and scored daily for disease signs according to the following 5-point clinical scoring criteria: 0: no disease; 0.5: tail weakness/partial limp tail; 1.0: full limp tail; 1.5: mild gait impairment; 2.0: severe gait impairment/hindlimb paresis; 2.5: partial hindlimb paralysis; 3.0: hindlimb paralysis/legs unable to paddle past hip; 3.5: hindlimb paralysis and forelimb paresis; 4.0: hindlimb paralysis and partial forelimb paralysis; 5.0: moribund or death.

Tamoxifen injection

Tamoxifen (20 mg/ml, Sigma Aldrich) was prepared in corn oil and allowed to dissolve at 37 °C overnight while shaking. Mice were injected i.p. with 2 mg tamoxifen on days indicated in Figure 3E.

Intracranial injections

Striatal injections were performed as previously described.[40–42] Mice were anaesthetized with 3% isoflurane; the head was shaved and placed in a stereotactic frame. A midline incision exposed the skull and a burr hole was drilled above the left striatum. A 1μL injection of murine recombinant IL-3 (rIL-3; 10 ng; Peprotech) was administered with a pulled glass capillary using the stereotactic coordinates: Anterior/Posterior, +1; Medial/Lateral, -2; and Dorsal/Ventral, -2.5. A 1 μL injection of sterile saline was used as a control. Post-injection, the capillary was held in place for one minute to limit backflow. The scalp was sutured, and animals were sacrificed 24 hours later.

Cells

Cell isolation

Peripheral blood was collected by retro-orbital bleeding, and erythrocytes were lysed in RBC lysis buffer (BioLegend, San Diego, CA). The spleen (SP), draining lymph nodes (LN), femurs, tibia, brain, and spinal cord (SC) were collected on ice after 20 ml vascular perfusion with cold PBS. Minced SP and LN and flushed bones were strained through 40 μm-nylon mesh (BD Biosciences) with PBS and further subjected to RBC lysis to generate single-cell suspensions of splenocytes, lymph nodes, and bone marrow (BM). Naive and inflamed SC were carefully removed by hydraulic extrusion with PBS and an 18 G needle. Fresh brains from intracranial injection experiments were dissected into 2 hemispheres and the injection site isolated for analysis. CNS tissue was minced and digested for 20 minutes in a thermomixer at 1000 rpm and 37°C in a 1 ml volume digestion mix of 450 U/ml collagenase I, 125 U/ml collagenase XI, 60 U/ml DNase I, 60 U/ml hyaluronidase, and 20 mM HEPES (Sigma-Aldrich) in PBS. After digestion, SC suspensions were strained using 70 μm-nylon mesh (BD Biosciences), mixed with a 30% Percoll/PBS solution, and a 70% Percoll/PBS solution was underlaid via disposable glass Pasteur pipette prior to centrifugation for 20 minutes at 690 x g and 25-26°C with the acceleration and brake remaining off. The upper cell fraction and mononuclear cell interface were collected and washed with room temperature PBS before downstream application.

Flow Cytometry and cell sorting

Single cell suspensions were stained in PBS supplemented with sterile 2% FBS and 0.5% BSA. The following monoclonal antibodies were used for flow cytometric analysis: anti-CD45 (clone 30-F11), anti-CD3 (clone 17A2), anti-CD3ε (clone 145-2C11), anti-CD4 (clone RM4-5), anti-CD8a (clone 53–6.7), anti-CD90.2 (clone 53-2.1), anti-CD19 (clone 6D5), anti-B220 (clone RA3-6B2), anti-Ly6G (clone 1A8), anti-Ly-6C (AL-21), anti-I-A/I-E (MHCII; clone M5/114.15.2), anti-CD11b (clone M1/70), anti-CD11c (clone HL3), anti-CD44 (clone IM7), anti-CD62L (clone MEL-14), anti-CD64 (clone X54-5/7.1), anti-CD80 (clone 16-10A1), anti-CD86 (clone GL-1), anti-OX40L (clone RM134L), anti-CD69 (clone H1.2F3), anti-CD49d (integrin α4; clone R1-2), anti-CD29 (integrin β1; clone HMβ1-1), anti-CXCR3 (CD183; clone CXCR3-173), anti-CCR6 (clone 29-2L17), anti-IL-3Rα (CD123; clone REA114), anti-F4/80

Please cite this article in press as: Kiss et al., Interleukin-3 coordinates glial-peripheral immune crosstalk to incite multiple sclerosis, Immunity (2023), https://doi.org/10.1016/j.immuni.2023.04.013

(clone BM8), anti-CD115 (CSF-1R; clone AFS98), anti-CX3CR1 (clone SA011F11), anti-IL-3 (clone MP2-8F8), anti-IFNγ (clone XMG1.2), anti-IL-17A (clone TC11-18H10.1), anti-GM-CSF (clone MP1-22E9), and anti-Ki67 (clone SolA15). All antibodies were used at a 1:200 dilution except for anti-IL-3 (1:166) and anti-CD123 (1:10). Antibodies were purchased from either BioLegend, BD Biosciences, eBioscience, or Miltenyi Biotec (Sunnyvale, CA). Viable cells were identified as unstained cells with Zombie Aqua™ (1:500-1:1000 dilution; BioLegend). For intracellular cytokine staining and analysis, cell suspensions were stimulated in 2% FBS RPMI-1640 medium with 50 ng/ml PMA and 500 ng/ml ionomycin (Sigma-Aldrich) in the presence of GolgiStop and GolgiPlug (each 1:2000; BD Biosciences) for 3.5-4 hours at 37°C, 5% CO_2 prior to viability staining with ZombieAqua plus Fc block with TruStain FcX™ (BioLegend) for 15 minutes at room temperature, extracellular antibody staining for 20 minutes at room temperature, fixation with BD Cytofix™ for 20 minutes at 4°C, and permeabilization for 30 minutes with BD Perm/Wash Buffer (BD Biosciences). Intracellular cytokine staining was performed in BD Perm/Wash Buffer for 45 minutes at room temperature. For Ki67 proliferation staining and analysis, cells were subject to viability staining with ZombieAqua™ plus Fc block with TruStain FcX™ (BioLegend) for 15 minutes at room temperature and extracellular antibody staining for 20 minutes at room temperature prior to fixation/permeabilization and intranuclear staining with the eBioscience™ Foxp3/Transcription. Factor Staining Buffer Set according to the manufacturer's instructions (ThermoFisher Scientific). Data were acquired on a BD LSRII and an Cytek Aurora Spectral cytometer and analyzed with FlowJo software (Tree Star, Ashland, OR). Cell sorting was conducted on a FACS Aria II or a Cytek Aurora cell sorter.

Ex vivo cell cultures

IL-3 production by tissular T cells

To analyze IL-3 production in T cells isolated from tissue, single-cell suspensions of roughly 2-5x10^6 cells per well were stimulated in 96-well flat-bottom plates in complete media for 20-24 hr in the presence of plate-bound anti-CD3ε (10 μg/ml) and soluble anti-CD28 (10 μg/ml) prior to intracellular cytokine staining (see staining strategies under *Flow cytometry* above).

T cell recall response

To analyze T cell proliferation and cytokine production in *Il3*$^{+/+}$ or *Il3*$^{-/-}$ mice in the peripheral compartment at the preclinical disease stage, spleens (n=3/group) were isolated on 8 dpi after subcutaneous MOG_{35-55}/CFA injection and cultured in the presence of increasing concentrations of MOG_{35-55} for 16 hours at 2-5x10^5 cells per well (with technical duplicates) prior to flow cytometry analysis and supernatants were collected for ELISA.

T cell/monocyte co-culture

For ex vivo T cell polarizations and monocyte co-culture, splenic $CD4^+$ T cells were isolated and polarized for differentiation into T_H subsets by exposing cells to the following cytokine cocktails: T_H1: IL-12 (20 ng/ml) and anti-IL-4 (10 μg/ml); "nonpathogenic" T_H17 (referred to as Th17(β)): recombinant human TGF-β1 (2 ng/ml; PeproTech), IL-6 (25 ng/ml), and anti-IL-4, anti-IL-12/23, and anti-IFN-γ (10 μg/ml each); and "pathogenic" T_H17 (referred to as Th17(23)): IL-23 (20 ng/ml), IL-1β (20 ng/ml), IL-6 (25 ng/ml), and anti-IL-4 and anti-IFN-γ (10 μg/ml each). After the 48 hr rest phase in IL-2, the indicated CD4+ T_H cell populations (1 × 105 cells/well for T_H1, T_H17(β) and T_H17(23)) were co-cultured with freshly isolated BM monocytes (1 × 105 cells/well), plate-bound anti-CD3ε (2 μg/ ml), soluble anti-CD28 (2 μg/ml) and T_H-polarizing cytokines for 24 hr in flat-bottom 96-well plates. Cell culture supernatant was collected for ELISA to assess CCL2 production.

SC myeloid cell sorting and qPCR

To analyze gene expression of myeloid cell chemoattractants from leukocytes in the inflamed spinal cord at the peak of disease (15 dpi), sorted leukocyte subsets (1x10^4 cells per well) were stimulated in 96-well flat-bottom plates with or without recombinant murine IL-3 (50 ng/ml; PeproTech) for 16 hours and subjected to mRNA isolation and qPCR as described below.

Mouse bone marrow (BM) monocyte culture

Femurs and tibias were collected from mice as described and processed into single-cell suspensions. BM monocytes were isolated by MACS magnetic depletion of non-monocytes via the Monocyte Isolation Kit (BM) (Miltenyi Biotec). BM monocytes were washed in PBS and further cultured in complete media at a concentration of 0.5-1x10^6 cells/ml in flat-bottom 96-well plates for up to 5 days recombinant murine IL-3 (PeproTech) at 20 ng/ml. Cells were then analyzed via flow cytometry or mRNA was isolated for downstream qPCR analysis.

Histopathology

Tissue processing and staining

Mice were euthanized under isoflurane anesthesia, perfused intracardially with 20 ml ice-cold PBS, and spinal columns were collected on-ice. Spinal cords were carefully removed by hydraulic extrusion with PBS and an 18 G needle (320). Then, spinal cords were divided into four sections and embedded in Tissue-Tek O.C.T. compound (Sakura Finetek, Torrance, CA), frozen in 2-Methylbutane (Fisher Scientific, Fair Lawn, NJ), cooled with dry ice, and serial frozen sections were prepared (7-μm slices).

Spinal cord demyelination analysis by Luxol fast blue (LFB) staining

Demyelination of spinal cords was analyzed by staining with LFB according to Luxol Fast Blue Stain Kit (Myelin Stain) manufacturer instructions (Cat. No. ab150675; Abcam) and counterstained with Cresyl Echt Violet Solution. Demyelinated areas were scanned using a digital slide scanner (NanoZoomer 2.0RS; Hamamatsu Photonics KK, Japan) and processed and analyzed using NDP.view 2 viewing software (Hamamatsu Photonics KK, Japan). Briefly, normalized demyelinated area (μm^2) was evaluated for each spinal cord vertebral region (i.e., cervical, thoracic, lumbar, and sacral) by normalizing the total area of gated white matter demyelinated regions of interest (ROIs) within a given section to the total area of each spinal cord tissue section analyzed. Percent demyelination for the

Please cite this article in press as: Kiss et al., Interleukin-3 coordinates glial-peripheral immune crosstalk to incite multiple sclerosis, Immunity (2023), https://doi.org/10.1016/j.immuni.2023.04.013

spinal cord of each mouse was calculated as follows: Percent demyelination = [Sum of the area of gated white matter demyelinated ROIs] ÷ [Sum of the total area of spinal cord tissue section analyzed] × 100.

Immunohistology for IL-3-producing cells and IL-3Rα+ cells in the central nervous system

An anti-IL3 antibody (1:5, 503902, MP2-8F8, BioLegend) followed by a biotinylated rabbit anti-rat IgG secondary antibody and streptavidin DyLight 594 (1:100, BA-4001 and 1:600, SA-5594, Vector Laboratories) were used for IL-3 detection. For co-localization of GFAP, AF488-GFAP antibody (1:50, 53-9892, eBioscience) was incubated at 4°C overnight. For co-localization of IL-3Rα with CD11b, an anti-Interleukin 3 Receptor Alpha antibody (1:50, 141039, US Biological) followed by an anti-CD11b antibody (1:25, 550282, M1/70, BD Biosciences) were incubated at 4°C overnight after blocking with 4% goat serum in PBS. A biotinylated goat anti-rabbit IgG secondary antibody (1:100, BA-1000, Vector Laboratories) and streptavidin DyLight 594 were used for IL-3Rα and a goat anti-rat IgG secondary antibody, Alexa Fluor 488 (1:100, A-11006, Thermo Fisher Scientific) were used for CD11b. All sections were counterstained with DAPI (1:3000, D21490, Thermo Fisher Scientific) and the slides were scanned using a digital slide scanner (NanoZoomer 2.0RS; Hamamatsu Photonics KK, Japan) and processed and analyzed using NDP.view 2 viewing software (Hamamatsu Photonics KK, Japan).

Molecular Biology

Quantitative PCR

Mouse total RNA was isolated using the RNeasy Mini Kit (Qiagen, Venlo, Netherlands) and ~10 mg tissue/sample according to the manufacturer's instructions. cDNA was generated from 1 μg of total RNA per sample using High Capacity cDNA Reverse Transcription Kit (Applied Biosystems, Foster City, CA). For cells, 5 × 10^3 Ly6C^{high} monocytes, moDC, MHCII^{high} macrophages, neutrophils, and microglia were sorted from inflamed spinal cord or harvested from cultured cells, and total RNA was extracted using the RNeasy Micro Kit (Qiagen) followed by cDNA transcription as described above. Quantitative PCR (qPCR) was performed using following TaqMan primers and their corresponding assay ID (Applied Biosystems): *Il3* (Mm00439631_m1), *Ccl2* (Mm00441242_m1), *Ccl5* (Mm01302427_m1), *Ccl7* (Mm00443113_m1), *Ccl12* (Mm01617100_m1), *Il3rα* (Mm00434273_m1), *Csf2rb* (Mm00655745_m1), *Ccr7* (Mm99999130_s1), *Flt3* (Mm00439016_m1), *Kit* (Mm00445212_m1), *Spp1* (Mm00436767_m1), *C5ar1* (Mm00500292_s1), *Irf4* (Mm00516431_m1), *Ly6c2* (Mm00841873_m1), *Cd209a* (Mm00460067_m1), *Fcgr1* (Mm00438874_m1), *Zbtb46* (Mm00511327_m1), and *Actb* (Cat. No. 4352341E; assay ID: Mm00607939_s1) as an endogenous control. qPCR was run on a 7500 thermal cycler (Applied Biosystems), and data were quantified with the $2^{-\Delta\Delta Ct}$ method.

ELISA

IL-3 was measured in serum, spinal cord tissue and cell culture supernatants with the Mouse IL-3 ELISA Kit (Boster Biological). Specifically for spinal cord tissue ELISA measurements, ~10 mg tissue/sample was homogenized in 0.3 ml RIPA buffer and left to sit for 10 minutes on ice, prior to microcentrifugation at 10,000 rpm for 8 minutes and collection of the supernatant. CCL2, IFNγ, IL17A, and GM-CSF were measured in culture media using ELISAs from R&D Systems and the manufacturer's instructions.

Human CSF proteomics

CSF samples were centrifuged at 400*g* for 10 minutes at room temperature. Cell-free supernatant was isolated and stored at -80°C until proteomics analysis, within 2 hours of collection. Leukocyte concentration was determined as per standard laboratory procedures (cells/μL). IL-3 concentration in CSF was determined using the SomaScan® platform from SomaLogic Inc, Boulder, Co., as previously described.[43] Data are presented in arbitrary units.

Human snRNAseq

Isolation and fluorescence-activated nuclear sorting (FANS) of nuclei for frozen human postmortem brain

Samples were processed in batches consisting of 2 individuals; 1 case and 1 control. For each case, we processed 3 dissections; 1 of gray matter, 1 white matter, and 1 containing an MS plaque. For each Control we processed 2 dissections; 1 gray matter and 1 white matter. Approximately 25 mg of frozen postmortem human brain tissue from each dissection was homogenized in cold lysis buffer (0.32M Sucrose, 5 mM CaCl2, 3 mM Magnesium acetate, 0.1 mM, EDTA, 10 mM Tris-HCl, pH8, 1 mM DTT, 0.1% Triton X-100) and filtered through a 40 μm cell strainer. All buffers were supplemented with RNAse inhibitors (Takara). The flow-through was underlaid with sucrose solution (1.8 M Sucrose, 3 mM Magnesium acetate, 1 mM DTT, 10 mM Tris-HCl, pH8) and centrifuged at 107,000 g for 1 hour at 4°C. Pellets were resuspended in PBS supplemented with 0.5% bovine serum albumin (BSA). Prior to FANS, volumes were brought up to 500 μl with PBS and DAPI (Thermoscientific) added to a final concentration of 1 μg/ml. DAPI-positive nuclei were sorted into tubes pre-coated with 5% BSA using a FACSAria flow cytometer (BD Biosciences).

Single-nuclei gene expression library preparation

Following FANS, nuclei were quantified (Countess II, Life Technologies) and 8,000 from each sample loaded on a single 10x lane using single cell 3' v3 reagents (10x Genomics). cDNA libraries were prepared according to the manufacturer's protocol. Libraries were sequenced at New York Genome Center using the Novaseq platform (Illumina).

Quantification of single-nuclei gene expression data

We used the cellranger (v.7.0.0) pipeline for preprocessing of the single-cell sequencing data. We aligned the fastq reads to the reference genome hg38, quantified the transcriptomic reads, and called cell barcodes to generate a feature-count-by-barcode matrix for subsequent analysis.

Please cite this article in press as: Kiss et al., Interleukin-3 coordinates glial-peripheral immune crosstalk to incite multiple sclerosis, Immunity (2023), https://doi.org/10.1016/j.immuni.2023.04.013

Clustering, annotation, and visualization of single-nuclei data

We used the pegasus (v1.7.0)[44] pipeline for QC and clustering, and scanpy (v1.9.1)[45] pipeline for visualization of the data. We first aggregated all 30 single-cell libraries and performed QC. We filtered out cells expressing less than 500 genes, less than 500 UMIs, and having mitochondrial gene fraction greater than 10 percent. After QC, we retained 77,490 cells for downstream analysis. We also filtered out genes expressed in less than 0.05% of all cells and retained 27,396 genes for analysis. The log-normalized counts were subjected to dimensionality reduction, and the first 25 PCs were used for clustering analysis. Since the single-cell libraries were prepared in 6 batches, we used Harmony[46] to correct for potential batch effect. We used Scrublet to filter out 2,315 cells predicted to be potential doublets from the data. Clustered cells were annotated based on marker genes defined in the pegasus pipeline. We used cell markers defined in both ''human_brain'' and ''human_immune'' to annotate 18 clusters. We used the Mann-Whitney U test for differential expression analysis by condition or clusters. For the cluster-based differential tests, we compared cells within the cluster with the rest of the cells. To count the cells expressing *IL3RA* (*IL3RA*$^+$ cells), we binarized the expression of *IL3RA* by cells expressing log-normalized expression greater than 1 (Figure S5B).

QUANTIFICATION AND STATISTICAL ANALYSIS

Results are shown as mean ± s.e.m. Statistical analysis was performed using GraphPad Prism 7 (Graphpad Software). Statistical tests included unpaired, two-tailed non-parametric Mann–Whitney *U*-tests (when Gaussian distribution was not assumed). For multiple comparisons, a non-parametric multiple-comparisons test comparing the mean rank of each group (when Gaussian distribution was not assumed) was used, or one- or two-way ANOVAs followed by Tukey's test were used. For correlation analysis, correlation was computed using Spearman correlation or Pearson correlation coefficients. *P value*s of 0.05 or less were considered to denote significance. Each experiment was repeated independently at least three times with similar results.